Geothermics 100 (2022) 102318

Contents lists available at ScienceDirect

Geothermics

journal homepage: www.elsevier.com/locate/geothermics

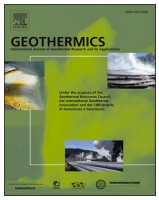

Techno-Economic Performance of Closed-Loop Geothermal Systems for Heat Production and Electricity Generation

Koenraad F. Beckers [a,b,*], Nicolás Rangel-Jurado [a], Harish Chandrasekar [a], Adam J. Hawkins [a], Patrick M. Fulton [a], Jefferson W. Tester [a]

[a] Cornell University, Ithaca, NY, USA
[b] Heateon, Gent, Belgium

ARTICLE INFO

Keywords:
Closed-Loop Geothermal
Advanced Geothermal Systems
Geothermal Reservoir Engineering
Slender-Body Theory for Transient Heat Conduction
COMSOL Multiphysics
Enhanced/Engineered Geothermal Systems

ABSTRACT

Closed-loop geothermal systems, recently referred to as advanced geothermal systems (AGS), have received renewed interest for geothermal heat and power production. These systems consist of a co-axial, U-loop, or other configuration in which the heat transfer or working fluid does not permeate the reservoir but remains within a closed-loop subsurface heat exchanger. Advocates indicate its potential for developing geothermal energy anywhere, independent of site-specific geologic uncertainties, and with limited risk of induced seismicity. Here, we present a technical and economic analysis of closed-loop geothermal systems using a Slender-Body Theory (SBT) model, COMSOL Multiphysics simulator, and the GEOPHIRES analysis tool. We consider a number of different scenarios and evaluate the influence of variations in reservoir temperature (100 to 500°C), well termination depth (2 to 4 km), mass flow rate (10 to 40 kg/s), injection temperature (10 to 40°C), fluid type (liquid water vs. supercritical carbon dioxide), design configuration (co-axial vs. U-loop), and degree of reservoir convection (natural, forced or conduction-only). The resulting average heat production rates range from about 2 to 15 GWh per year for cases considering a co-axial design and from 9 to 67 GWh per year for cases with a U-loop design. Assuming generous economic and operating conditions, estimates of levelized cost of heat range from ~$20 – $110 per MWh (~$6 – 32/MMBtu) and ~$10 – $70 per MWh (~$3 – $20/MMBtu) for greenfield co-axial and U-loop cases, respectively. In the scenarios in which electricity generation is considered, annual electricity production ranged between 0.12 and 7.5 GWh per year at a levelized cost of electricity from roughly $83 to $2,200 per MWh. In all scenarios, the results exhibit a large rapid drop in production temperature after initiation of operations that levels off to a steady value significantly below the initial reservoir temperature. Operating at lower flow rate increases the production temperature but also lowers the total heat production. The consistently low production temperatures hinder efficient electricity generation in most cases considered. Natural or forced convection can increase thermal output but requires sufficiently high reservoir permeability or formation fluid flow. As expected, overall system costs are heavily dependent on drilling costs; hence, repurposing existing wells could significantly lower capital and levelized costs. In comparison with other types of geothermal systems, our results for closed-loop geothermal systems predict long-term production temperatures considerably below the initial reservoir temperature, and relatively high levelized costs for greenfield closed-loop geothermal systems, particularly for electricity production, unless significant reductions in drilling costs are obtained.

1. INTRODUCTION

Although the geothermal resource base is vast — the accessible thermal energy stored in the upper continental crust is several orders of magnitude larger than the annual global primary energy demand (Armstead and Tester, 1987; Rybach et al., 2000) — current installed geothermal electric and thermal capacity is relatively small. As of 2019,

Abbreviations: COM, COMSOL, CXA, Co-axial configuration with injection in annulus; CXC, Co-axial configuration with injection in center pipe; EGS, engineered/enhanced geothermal system; GEOPHIRES, GEOthermal energy for Production of Heat and electricity ("IR") Economically Simulated; LCOE, Levelized Cost of Electricity; LCOH, Levelized Cost of Heating; ORC, Organic Rankine Cycle; SBT, Slender Body Theory; sCO2, Supercritical Carbon Dioxide; U1, U-Loop with one lateral section; U2, U-Loop with two lateral sections; U5, U-Loop with five lateral sections; U13, U-Loop with thirteen lateral sections.

* Corresponding author: Dr. Koenraad Beckers, Cornell University, Ithaca NY 14853, USA
E-mail address: kb447@cornell.edu (K.F. Beckers).

https://doi.org/10.1016/j.geothermics.2021.102318
Received 4 June 2021; Received in revised form 26 October 2021; Accepted 11 December 2021
Available online 31 December 2021

LIST OF SYMBOLS

a	Geothermal Gradient [°C·m^{-1}]
$C_{p,f}$	Specific Heat Capacity of Fluid [J·kg^{-1}·K^{-1}]
d	Hydraulic diameter of pipe [m]
f	Darcy friction vector [-]
$f(t)$	Ramey Time Function
$f_{i,j,m,n}$	Temperature change at element i at the end of time step m as a result of the heat pulse at element j during time step n.
g	Acceleration due to gravity [9.81 m·s^{-2}]
H	Height of Fracture [m]
h	Convective heat transfer coefficient [W·m^{-2}·K^{-1}];Specific Enthalpy [J·kg^{-1}]
k_r	Rock Thermal Conductivity [W·m^{-1}·K^{-1}]
$\dot{m}$	Mass flow Rate [kg·s^{-1}]
p	Fluid Pressure [Pa]
Q	Heat Exchange between fluid and the rock [W·m^{-1}]
$Q_{j,n}$	Heat Pulse at element j during time step n [W·m^{-1}]
R_t	Thermal Resistance [W·m^{-1}·K^{-1}]
r_i	Inner radius of the pipe [m]
r_o	Outer radius of the pipe [m]
r_{co}	Casing Outer Radius [m]
T_0	Tock temperature at the inlet [°C]
T_f	Fluid Temperature [°C]
T_i	Fluid temperature at inlet [°C]
$T_{i,m}$	Temperature in each pipe element i at the end of time step m [°C]
T_r	Rock Temperature [°C]
t	Time [s]
U	Overall Heat Transfer Coefficient [W·m^{-2}·K^{-1}]
v	Fluid Velocity [m·s^{-1}]
W	Width of Fracture [m]
z	Local axial coordinate along the heat exchanger in the flow direction [m]
α_r	Rock Thermal Diffusivity [m^2·s^{-1}]
θ	Angle made by the fluid flow direction with the horizontal [deg]
ρ	Fluid Density [kg·m^{-3}]

installed worldwide capacity is limited to roughly 16 GW_e in electricity production (Huttrer, 2020) and 30 GW_{th} in direct-use heat systems (excluding ground-source or "geothermal" heat pumps) (Lund and Toth, 2020). Most systems today produce fluids from highly-permeable, high-temperature reservoirs, also referred to as hydrothermal systems, which are geographically limited and scarce. Much more common are formations where heat is present, but in-situ fluids are lacking or natural permeability is low, hindering profitable production. Efforts to utilize these unconventional geothermal systems are referred to as enhanced geothermal systems (EGS), and often involve the stimulation of fluid flow pathways within the bulk rock using hydraulic, chemical and thermal techniques that create or re-open existing fracture networks. Although technical feasibility has been demonstrated at several sites, challenges remain for EGS to become a reliable and financially-appealing approach to harness geothermal energy on a global scale.

1.1. Closed-Loop Geothermal Systems

Another approach for extracting heat from low-permeability formations is utilizing closed-loop geothermal systems. With these systems, the heat transfer or working fluid (e.g., water or supercritical CO_2 (sCO_2)) does not permeate the reservoir. Instead, fluids circulate through a closed-loop wellbore system that exchanges heat with the surrounding bulk rock. Although closed-loop designs have been proposed for nearly a century (Hodgson, 1927), they have recently received considerable attention and commercial investment and have been referred to as Advanced Geothermal Systems (AGS). Proponents of AGS indicate that no reservoir stimulation is required, lowering the risk of induced seismicity and avoiding the technical challenge of creating a set of fractures with sufficient area and without short circuits. Other benefits are that AGS can be applied to repurpose abandoned or ill-producing wells, or extract heat from a reservoir without producing reservoir fluids to avoid challenging fluid chemistry or insufficient subsurface fluid pressures. However, AGS introduces new challenges such as obtaining sufficient contact area with the rock for sustained and acceptable rates of heat extraction, as well as the need in certain designs to drill and connect multiple loops of horizontal wells at acceptable costs.

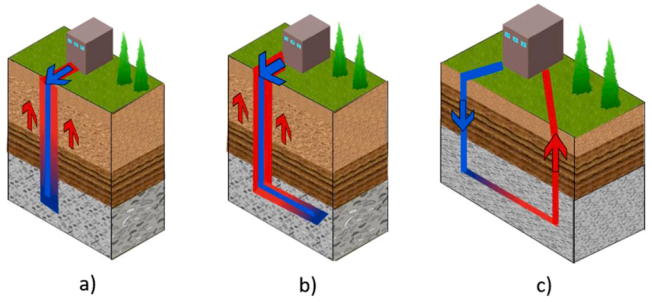

Fig. 1. Common AGS designs with fluid color in wells representing arbitrary temperature (blue = cold; red = hot). a) Vertical co-axial or "pipe-in-pipe" system with insulation (e.g., vacuum insulated tubing) between annulus and center pipe. Diagram shows cold fluid injection in the annulus and hot fluid production through the center pipe; certain designs consider reverse flow; b) Co-axial system similar to a) but with horizontal extension; c) U-loop system with injection in one well, production through a second well, and one or multiple horizontal laterals connecting the two wells. Schematics are not to scale. (For interpretation of the references to colour in this figure legend, the reader is referred to the web version of this article.)

Significant debate remains on feasibility, performance and cost-competitiveness of AGS. Various claims have been made in literature and industry regarding their cost and output, but underlying assumptions are not always reported. In some circumstances, no clear distinction is made between heat and electricity, for example. In others, reported performances appear to be unrealistically favorable. With various assumptions for subsurface and operating conditions, comparing designs and determining the ideal system for a certain resource is challenging. With recent uptake in interest and investment in closed-loop geothermal, a careful and independent evaluation of the techno-economic performance of these systems is both timely and desirable. Here, we address this outstanding need by evaluating the techno-economic performance of a variety of potential AGS wellbore designs, configurations, and operating conditions, and calculate corresponding values for levelized cost of heat (LCOH) and levelized cost of electricity (LCOE). Using a combination of an analytical model, a finite element numerical simulator, a reservoir heat transfer simulator based on the Slender Body Theory (SBT), and the GEOPHIRES techno-economic simulator, we determine the thermal output, electricity production, and estimated capital and levelized costs of heat and electricity. Through our analysis, we systematically explore the influence of several parameters including depth, reservoir temperature, reinjection temperature, and mass flow rate. In addition, the potential advantage of convective and/or advective heat transfer from in-situ fluids surrounding the closed-loop is quantitatively assessed.

Table 1
AGS studies reviewed in literature, summarizing the AGS type considered, the bottom-hole temperature, AGS depth, AGS horizontal length (if applicable), fluid type, fluid flow rate, and major findings on techno-economic performance.

Study	AGS Type	Bottom-hole Temp-erature	AGS Depth	AGS Horizontal length	Flow Rate	Fluid type	Findings on techno-economic performance
Horne (1980)	Co-axial	100°C	200 m	N/A	1 to 40 $kg{\cdot}s^{-1}$	Water	5 to 60 kW_{th} of heat production
Morita and Tago (1995) and Morita et al. (2005)	Co-axial	260 to 320°C	2 km	N/A	11 to 21 $kg{\cdot}s^{-1}$	Water	Heat output on the order of 1 MW_{th} converting to 50 to 100 kW_e of electricity
Bobok et al. (2007)	Co-axial	120°C	2 km	N/A	1 to 15 $kg{\cdot}s^{-1}$	Water	Long-term production temperatures in the range 25 to 65°C (higher temperature for lower flow rate) and thermal power in the range 200 to 350 kW_{th} (higher power for higher flow rate)
Nalla et al. (2005)	Co-axial	350°C	5.6 km	N/A	1.3 to 32 $kg{\cdot}s^{-1}$	Various	Maximum electricity production of 50 kW_e
Riahi et al. (2017)	Co-axial	240°C	2.5 km	1.1 km	60 $kg{\cdot}s^{-1}$	Water	Heat production on the order of 3 MW_{th}
(Xu et al., 2020)	Co-axial	77°C	2.8 km	N/A	15 to 30 $kg{\cdot}s^{-1}$	Water	Production temperatures in the range 35°C to 55°C, and heat production in the range 300 kW_{th} to 700 kW_{th}; Porosity and permeability have negligible impact on the performance; Intermittent operation results in higher heat production during circulation
Fox and Higgins (2016)	Co-axial	680°C	5.5 km	N/A	Not reported	sCO_2	1 MW_e of power production over 25 year lifetime; Minimum 100 m of well spacing limits the degradation due to thermal interference between the wellbores
Higgins et al. (2019); Amaya et al. (2020; 2021)	Co-axial with brine flow in annulus	Local gradient of 120°C·km^{-1}	330 m	N/A	23 to 30 $kg{\cdot}s^{-1}$ for water; 1.5 to 5.5 $kg{\cdot}s^{-1}$ for sCO_2	Water and sCO_2	Demonstration of GreenFire Energy system at Coso geothermal field; Tests validated their models and indicate power production up to 1.2 MW_e. sCO_2 tests solely driven by thermosiphon effect with power production in the range 5 to 30 kWe.
Scherer et al. (2020)	Co-axial	~500°C	4 km	4 km	Not reported	sCO_2	Power production of 1 MW_e assuming thermal conduction-only in the reservoir
Oldenburg et al. (2016)	U-loop	250°C	2.5 km	1.1 km	6 to 90 $kg{\cdot}s^{-1}$	Water and sCO_2	Estimated enthalpy gains in the range 1 to 6 MW; Low injection temperatures and high reservoir permeability significantly increase the energy gain
Riahi et al. (2017)	U-loop	240°C	2.5 km	1.1 km	60 $kg{\cdot}s^{-1}$	sCO_2	Enthalpy gain around 2 MW
Esmaeilpour et al. (2021)	U-loop	130°C	4 km	4 km	1 to 10 $kg{\cdot}s^{-1}$	Water	Heat production on the order of 2 MW_{th} for 5 $kg{\cdot}s^{-1}$ flow rate
Malek et al. (2021)	U-loop	138°C	3.5 km	4 loops of 5 km each	27 $kg{\cdot}s^{-1}$ for water and 53 $kg{\cdot}s^{-1}$ for CO_2	Water and CO_2	Optimal net electricity generation of 174 kW_e for water as heat transfer fluid and 313 kW_e for CO_2; Capital costs estimated at $136M for the water-based system ($785,000/$kW_e$) and $156M for the CO_2-based system ($498,000/$kW_e$).
Zhang et al. (2021)	U-loop	45 to 95°C	2.5 km	450 m	17 to 33 $kg{\cdot}s^{-1}$	Water	Heat production in the range 600 to 1,300 kW_{th}
Van Oort et al. (2021)	U-loop	222°C	7 km	7 km	97 $kg{\cdot}s^{-1}$	Water	Heat production during first 20 hours on the order of 50 MW_{th}; We conducted Long-term simulations for this design (see Appendix A5) and found that heat production would quickly drop and average about 5 MW_{th} over a 20 year lifetime.
Vany et al. (2020); (Eavor 2021)	U-loop	75°C	2.4 km	2 laterals of 2 km each	Not reported	Not reported	Demonstration project of Eavor-Loop technology in Alberta, Canada; Thermal output on the order of 800 kW_{th}.

1.2. Literature Review

Various closed-loop configurations have been proposed, including a co-axial ("pipe-in-pipe") wellbore heat exchanger in a vertical well (Fig. 1a) and in a vertical well with horizontal extension (Fig. 1b), and a U-loop piping configuration where one or several long horizontal heat exchangers connect an injection well to a production well (Fig. 1c). AGS do not require reservoir permeability (either through the rock matrix or a fracture network) nor naturally-occurring reservoir fluids for their operation. However, in conduction-dominated reservoirs, limited contact area between the boreholes and the host rock, and low rock thermal conductivity and diffusivity, limit the rate of heat production these systems can provide. The relatively slow rate of replenishment of thermal energy extracted in the vicinity of the wellbore hinders achieving high thermal performance over a long time period (Wang et al., 2010; Cheng et al., 2013; Wang et al., 2021). Certain designs attempt to overcome this limitation by employing multiple closed-loop heat exchangers in parallel to increase the heat transfer contact area with the rock, or by targeting very hot reservoirs, where high rock temperatures cause steep temperature gradients and partially compensate for limited heat transfer area. Other designs propose developing AGS in hot and permeable sedimentary aquifers, where fluid flow—either gravity-driven or forced—may sufficiently fast replenish depleted heat surrounding the borehole. Some designs propose hybrid AGS/EGS configurations involving convective fluid flow in existing or created fractures in the rock. Some systems focus on power production and circulate the working fluid directly in the closed-loop heat exchanger. AGS has also been proposed to repurpose idle or abandoned (but not plugged) geothermal, oil or gas wells and in areas where hydraulic stimulation is banned. In certain cases, idle wells in existing geothermal fields may be unable to produce fluid due to reservoir hydraulic drawdown constraints, permit limitations, presence of high levels of non-condensable gases, or aggressive fluid chemistry that could result in scaling or corrosion. AGS has been proposed for such wells to deliver heat to the surface without fluid extraction from the reservoir.

Over the last several decades, a number of studies have been conducted to investigate AGS designs for particular wellbore geometries, reservoir conditions, and operating conditions (Table 1). These studies generally provide anticipated production temperatures, and in some cases, reservoir heat extraction and power production levels based on a

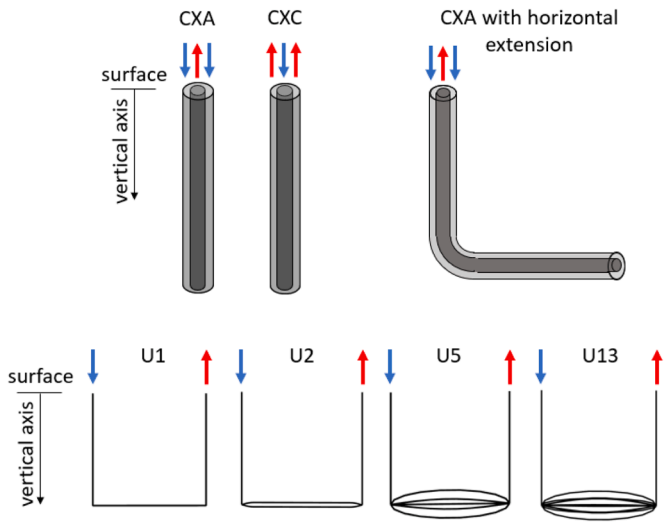

Fig. 2. Schematic representation of AGS configurations studied. Co-axial cases include injection in the annulus (CXA) and in the center pipe (CXC), as well as one CXA with a horizontal extension. U-loop cases include one lateral (U1), two laterals (U2), five laterals (U5) and thirteen laterals (U13). Arrow indicates injection (blue) and production (red) of fluid. Diagrams are not to scale. (For interpretation of the references to colour in this figure legend, the reader is referred to the web version of this article.)

variety of assumptions and modeling approaches. The assumptions and results of many of these studies are summarized in Table 1. Co-axial or U-loop AGS designs are considered in most studies and results are largely based on model simulations, although a few involve field observations from demonstration sites.

Review of these AGS studies reveals a wide range in estimated performance, from 10's of kW to 10's of MW in energy production, depending on design, depth, flow rate, bottom-hole temperature, etc. However, systematic comparison among studies to deduce optimal systems or find trends is non-trivial as underlying assumptions and results vary widely. In a few cases, it is not clear whether reported output power estimates refer to heat or electricity. Common findings, however, do include a rapid drop in production temperature before leveling off to a near steady-state temperature, and relatively low production temperatures in many cases, which hinder effective power production with a heat-to-electricity conversion cycle. For generating electricity, some studies suggest that sCO_2 may have promise as working fluid with AGS (*Oldenburg et al.,2016*; Fox et al., 2016; Scherer et al., 2020). Only limited economic results are reported in literature, which indicate relatively high costs, but comparisons with performance of traditional geothermal systems or EGS are generally not included.

2. STUDY OBJECTIVE AND OUTLINE

Here using a common approach and careful sensitivity analysis we conduct a systematic evaluation of the technical performance and cost-competitiveness of closed-loop geothermal systems for heat production and electricity generation for a variety of designs, operational configurations, and subsurface conditions. We consider both co-axial and U-loop designs, and investigate the impact of different depths, temperatures, permeabilities, flow rates, and injection temperatures on system performance. We also consider both water and sCO_2 as heat transfer/working fluids, and consider the influence of natural or forced convection. Using validated numerical models, we simulate and assess subsurface heat extraction with closed-loop systems over a 20-year lifetime and compare results with reported performance for existing hydrothermal systems. We also conduct a first-order economic analysis to estimate capital costs, and LCOH and LCOE values, which we also compare to the economics of traditional geothermal systems.

In Section 3 we describe our approach. AGS heat transfer simulations are conducted with a transient heat conduction simulator based on a slender-body theory (SBT) model (Beckers et al., 2015) implemented in MATLAB (*MathWorks, 2020*) and the finite element numerical simulator COMSOL Multiphysics®□ (COMSOL, 2019), and economic performance is evaluated using the GEOPHIRES v2.0 techno-economic assessment tool (Beckers and McCabe, 2019). In Section 4 we present and discuss the results of a wide range of different case scenarios that allow us to assess the influence of different parameters on produced temperature, heat and electricity, and overall economics. We then discuss the implications of these results and present summary conclusions in Section 5. As appendices, we also provide a detailed description of the SBT model in Appendix A1 and multiple model validations in Appendices A2-A4. In Appendix A5 we also present a much longer-term assessment of a deep U-loop configuration previously considered with intriguing results by Van Oort et al. (2021) for short timescales.

3. METHODOLOGY

Based on the range of designs presented in the literature (Table 1; Section 1.2), we consider two different styles of AGS: co-axial and U-loop systems. For the co-axial cases, we consider both a wellbore that is entirely vertical to the target depth and an alternative case where a long, horizontal section is extended at the bottom of the vertical section (Fig. 2). For the U-loop cases, we consider configurations with a number of horizontal laterals ranging from one to thirteen (Fig. 2). For both the co-axial and U-loop designs, we simulate several cases to allow for investigation of the thermal and economic performance over a 20-year lifetime for a variety of subsurface temperatures ranging from 100 to 500°C, injection temperatures ranging from 10 to 40°C, and mass flow rates ranging from 10 to 40 $kg{\cdot}s^{-1}$. In addition, we consider different fluid types (water or sCO_2), and reservoirs with and without convection. In total, we evaluate 34 cases for direct-use heating and 6 cases for electricity generation.

We conduct reservoir heat transfer simulations using three different model frameworks: (1) a hybrid numerical-analytical model using Slender-Body Theory (SBT) (Beckers et al., 2015); (2) a numerical finite element solver using the commercial COMSOL software; and (3) a simple, analytical solution for wellbore heat transmission (Ramey, 1962). These three models vary in ease-of-use, computational efficiency, and capabilities. The analytical model by (Ramey, 1962) is an easy-to-use analytical solution that provides rapid estimation of the long-term performance of a straight heat exchanger in a conduction-only reservoir (see Appendix A2), whereas COMSOL is a computationally-intensive simulator able to handle various AGS configurations and reservoir conditions, requiring more user experience. The SBT model represents an intermediate approach which provides accurate simulations in a computationally-efficient fashion. Both SBT and COMSOL are employed to simulate the co-axial AGS cases in conduction-only reservoirs. For the U-loop cases in conduction-only reservoirs, we predominantly use the SBT model with the COMSOL and Ramey models providing validation. The natural convection cases are simulated with COMSOL, while the forced convection cases are simulated with the SBT model. The physical properties, dimensions, initial and boundary conditions, and other assumptions are presented along with the results for each particular case scenario in Section 4. To validate our models, we simulate multiple AGS cases with SBT, COMSOL and the Ramey model. These validation results are presented in Appendices A2, A3, and A4.

3.1. Slender-Body Theory (SBT)

The SBT model is a hybrid model that discretizes the wellbore numerically but solves heat transfer between the wellbore and the rock using analytical equations based on Green's functions. The model was originally developed by Beckers et al. (2015) for transient heat transfer

Table 2
Co-axial AGS cases simulated to investigate impact of reservoir temperature. Heat transfer within reservoir is through heat conduction only. Case 1 represents the co-axial AGS base case. The changes with respect to the base case are highlighted in bold. CXA = co-axial with injection in annulus; SBT = Slender Body Theory Model; COM = COMSOL Model.

Case No.	AGS Type	Reservoir Temperature (°C)	Reservoir Depth (km)	Lateral Length (km)	Injection Temperature (°C)	Flow Rate ($kg{\cdot}s^{-1}$)	Fluid	Simulator
1	CXA	200°C	2 km	0 km	20°C	20 $kg{\cdot}s^{-1}$	Water	SBT/ COM
2	CXA	**150°C**	2 km	0 km	20°C	20 $kg{\cdot}s^{-1}$	Water	SBT/ COM
3	CXA	**300°C**	2 km	0 km	20°C	20 $kg{\cdot}s^{-1}$	Water	SBT/ COM
4	CXA	**500°C**	2 km	0 km	20°C	20 $kg{\cdot}s^{-1}$	Water	SBT/ COM

simulations with U-loop type heat exchangers with only heat conduction in the reservoir, and water with constant thermo-physical properties as heat transfer fluid. The model was updated for the present work to account for pipe-in-pipe configurations, multiple horizontal laterals, other heat transfer fluids than water, variable fluid properties as a function of pressure and temperature, and forced uniform water flow in a permeable reservoir. The SBT model can simulate multiple, curved and thermally-interacting heat exchangers in reservoirs with conduction-only heat transfer or forced uniform convection, but not natural convection. The SBT model obtains fast computational times on the order of a few seconds as a result of (1) the use of a hybrid approach only requiring a one-dimensional discretization along the heat exchanger instead of a full three-dimensional discretization of the reservoir domain, (2) further simplification of the analytical reservoir heat transfer equations by taking advantage of the slenderness of the heat exchanger and the large spatial extent of the reservoir (e.g., in certain cases, a cylindrical source can become a line source, a point source, or can even be neglected), and (3) incorporating the fast multipole method (Greengard and Rokhlin, 1987) to combine point sources in space and time. More information on the SBT model is provided in Appendix A1.

3.2. COMSOL Multiphysics

The software COMSOL Multiphysics v5.5 (COMSOL, 2019) is a commercial finite element numerical simulator and is used in this study to provide validation for the SBT simulations and to simulate vertical co-axial and U-Loop configurations in the presence of natural convection in the reservoir. Vertical co-axial AGS configurations are implemented using a two-dimensional axisymmetric model that solves for the coupled fluid flow and heat transport in the heat exchanger, within the rock formation, and in between. The element height (axially) is kept constant at 50 m; the element width varies radially and starts at 0.05 m close to the wellbore with a total of ~2500 mesh elements. Computation time for simulations with this model is on the order of 1 to 2 minutes. In contrast, U-loop configurations require a full three-dimensional implementation, resulting in simulation times of several hours with several million tetrahedral mesh elements.

3.3. GEOPHIRES

Potential for electricity generation is estimated using GEOPHIRES v2.0. When water is used as a circulating fluid, heat is converted to electricity using an Organic Rankine Cycle (ORC) power plant. Exergy is calculated for the produced fluid combined with a utilization efficiency reflecting the conversion from exergy to electricity. In case of sCO_2, the fluid directly drives a turbine to generate electricity. GEOPHIRES v2.0 was also used to perform a high-level economic assessment and estimate the LCOH and LCOE for produced heat and electricity, respectively.

4. RESULTS AND DISCUSSION

4.1. Overview of Simulated AGS Cases

In our assessment, we consider 40 AGS cases. Details of the assumptions and results of the different cases are presented in the following subsections and presented in a manner that allows for the influence of various factors or conditions to be assessed. About half of the cases assume a co-axial configuration (Fig. 2), most of them with fluid injection in the annulus (CXA). One co-axial case considers fluid injection in the center pipe (CXC), and one case assumes a CXA design with a horizontal extension. The remaining cases assume a U-loop configuration with one (U1), two (U2), five (U5), or thirteen (U13) horizontal laterals (Fig. 2), branching out from a single injection well and single production well. We first assess the thermal performance of AGS in conduction-only reservoirs (Section 4.2), followed by AGS thermal performance in reservoirs with natural and forced convection (Section 4.3). Section 4.4 presents simulation results considering electricity production. AGS capital and levelized cost estimates are discussed in Section 4.5.

All 40 cases assume: (1) temperature at ground surface is 20°C; (2) rock thermal conductivity is uniformly 2.83 $W{\cdot}m^{-1}{\cdot}K^{-1}$; (3) the bulk rock density is 2,875 $kg{\cdot}m^{-3}$; and (4) the specific heat capacity of the bulk rock is 825 $J{\cdot}kg^{-1}{\cdot}K^{-1}$. For CXA and CXC, the inner radius of the center pipe is 0.0635 m (5-inch inner diameter), the thickness of the pipe is 0.0127 m (0.5 inch), and the thermal conductivity of the pipe material (assuming vacuum insulation) is 0.006 $W{\cdot}m^{-1}{\cdot}K^{-1}$. The well radius for the co-axial systems is 0.1143 m (9-inch diameter). The thermal influence of the casing material and the annulus-filling cement are assumed negligible. All cases assume continuous operation (i.e., with utilization factor of 100%) over a 20-year lifetime. The U-loop cases assume a constant radius of 0.0762 m (6-inch diameter) for the vertical wells and horizontal laterals, neglecting the thickness of tubing, casing and cement (i.e., an "open hole" well completion). The U2 scenario has a 200 m spacing between the two laterals. In the U5 scenario, there is one straight lateral and four gently curved laterals (uniformly distributed) spaced 250 m from the center lateral at the midpoint. In the U13 scenario, there are one straight lateral, eight gently curved laterals (uniformly distributed) spaced 125 m from the center lateral at the midpoint, and four gently curved laterals (uniformly distributed) spaced 250 m from the center lateral at the midpoint. Four cases consider sCO_2 instead of water and assume high injection temperature (40°C) and high injection pressure (10^7 Pa) to ensure operation above the critical point of CO_2 (31°C; $74{\cdot}10^5$ Pa). Cases with natural convection assume an isotropic porosity of 5% and pore compressibility of $7.25{\cdot}10^{-12}$ Pa^{-1}.

For the cases with conduction-only in the reservoir (Section 4.2), parameters such as reservoir temperature (150 to 500°C), injection temperature (10 to 40°C), flow rate (10 to 40 $kg{\cdot}s^{-1}$), and working fluid (water or sCO_2) are varied to determine their impact on thermal performance. Other parameters are kept constant in each simulation, however, others have shown they could have a significant impact on system performance. For example, bulk rock thermal conductivity

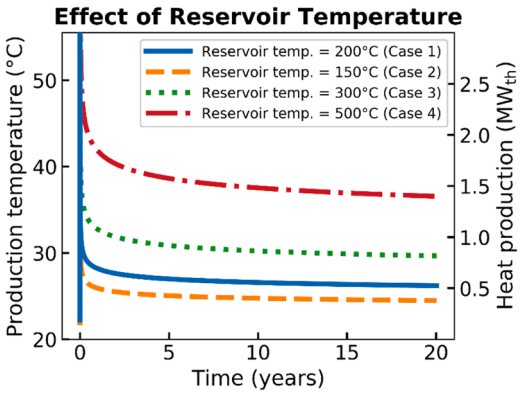

Fig. 3. Co-axial AGS simulation results for production temperature (°C) and produced heat (MW_{th}) for different reservoir temperature. Case 1 represents base case with reservoir temperature of 200°C. Cases 2 through 4 consider different reservoir temperature and depth. The base case yields long-term heat production of 0.57 MW_{th} with long-term production temperatures about 7°C above the injection temperature. All cases assume CXA configuration, reservoir depth of 2 km, and water as heat transfer fluid with flow rate of 20 $kg{\cdot}s^{-1}$ and injection temperature of 20°C.

ranges from roughly 1 to 7 W/m-K (Robertson, 1988); larger values tend to increase production temperatures and heat production (Esmaeilpour et al., 2021; Xu et al., 2020). In each case, a linear initial temperature profile (i.e., constant geothermal gradient) was assumed in the reservoir domain with 20°C at the surface and a certain reservoir temperature at a specific depth. For example, Case 1 assumes 200°C at 2 km depth, corresponding to a geothermal gradient of 90°C/km.

4.2. AGS thermal performance with heat conduction-only in reservoir

4.2.1. Co-axial AGS thermal performance in conduction-only reservoirs

4.2.1.1. Base case and impact of reservoir temperature. As a base case co-axial AGS design we consider a 2 km vertical well and 200°C reservoir temperature, operating with water as the heat transfer fluid at an injection temperature of 20°C and flow rate of 20 $kg{\cdot}s^{-1}$ (Table 2). The solid blue curve in Fig. 3 illustrates the results of production temperature and heat production over time. As observed in previous studies, values are relatively high immediately after the start of operation, but then rapidly fall to much lower values. For this base case scenario, the average production temperature is ~27°C (7°C above the injection temperature), corresponding to ~0.57 MW_{th} of heat. These relatively low production temperatures on the order of 20°C to 60°C — as observed for many of the cases studied in Section 4.2 — are too low for electricity generation and are therefore only considered for direct-use heating. Different scenarios are investigated in Section 4.4 for electricity generation (including higher reservoir temperatures and lower flow rates, which result in higher production temperatures).

The dashed and dotted orange, green and red curves in Fig. 3 show the results from similar cases (2, 3, and 4) but with reservoir temperature of 150°C, 300°C, and 500°C, respectively. The relationship between reservoir temperature and thermal output (production temperature and heat production) is linear. For a reservoir temperature of 150°C, average heat production is on the order of 0.4 MW_{th} compared to 0.6 MW_{th} for 200°C, 0.9 MW_{th} for 300°C, and 1.5 MW_{th} for 500°C.The "low-temperature" scenario with 150°C at 2 km depth (Case 2) corresponds to a medium-grade resource with geothermal gradient of 65°C/km. Scenarios with lower reservoir temperatures would result in even lower thermal performance and are not further considered in this study.

4.2.1.2. Impact of depth in co-axial systems. Because one of the primary means of targeting higher reservoir temperature is to drill deeper, we also consider the influence of depth on thermal performance (Table 3, Fig. 4). Keeping the reservoir temperature 200°C but adjusting the depth at which it occurs (at 3 km in Case 5; at 4 km in Case 6), we find an approximate linear increase of long-term heat production with depth. For a 3 km deep co-axial AGS system (Case 5), the heat production increases to 0.85 MW_{th}; for a 4 km deep system (Case 6), the long-term heat production is 1.1 MW_{th}. Although the reservoir temperature is the same in these cases, increasing the heat exchanger area results in an increase in production temperature and heat production.

4.2.1.3. Impact of injection temperature in co-axial systems. Whereas Sections 4.2.1.1 and 4.2.1.2 demonstrate the influence of the reservoir, we now investigate operational considerations for co-axial systems, including injection temperature, flow rate and fluid type. We start with cases 7 and 8 that keep the same parameterization as the co-axial base case (Case 1), but have injection temperatures of 10 and 40°C rather than 20°C (Table 4). Fig. 5 illustrates that a lower injection temperature results in lower production temperatures but larger temperature gains (i.e., difference between injection and production temperature. The

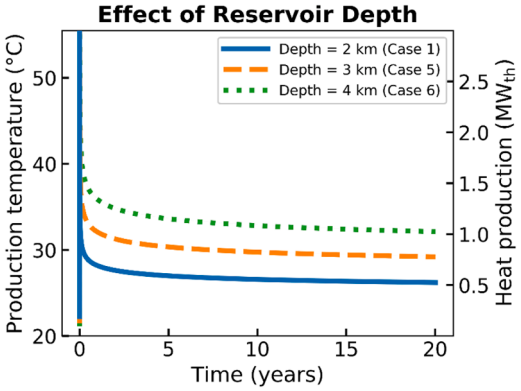

Fig. 4. Co-axial AGS simulation results for production temperature (°C) and produced heat (MW_{th}) for different reservoir depth. Case 1 represents base case with reservoir temperature of 200°C. Cases 5 through 6 consider different reservoir depths. All cases assume CXA configuration, reservoir temperature of 150°C, and water as heat transfer fluid with flow rate of 20 $kg{\cdot}s^{-1}$ and injection temperature of 20°C.

Table 3
Co-axial AGS cases simulated to investigate impact of reservoir depth. Heat transfer within reservoir is through heat conduction only. Case 1 represents the co-axial AGS base case. The changes with respect to the base case are highlighted in bold. CXA = co-axial with injection in annulus; SBT = Slender Body Theory Model; COM = COMSOL Model.

Case No.	AGS Type	Reservoir Temperature (°C)	Reservoir Depth (km)	Lateral Length (km)	Injection Temperature (°C)	Flow Rate ($kg{\cdot}s^{-1}$)	Fluid	Simulator
1	CXA	200°C	2 km	0 km	20°C	20 $kg{\cdot}s^{-1}$	Water	SBT/COM
5	CXA	200°C	**3 km**	0 km	20°C	20 $kg{\cdot}s^{-1}$	Water	SBT/COM
6	CXA	200°C	**4 km**	0 km	20°C	20 $kg{\cdot}s^{-1}$	Water	SBT/COM

Table 4
Co-axial AGS cases simulated to investigate impact of injection temperature. Heat transfer within reservoir is through heat conduction only. Case 1 represents the co-axial AGS base case. The changes with respect to the base case are highlighted in bold. CXA = co-axial with injection in annulus; SBT = Slender Body Theory Model; COM = COMSOL Model.

Case No.	AGS Type	Reservoir Temperature (°C)	Reservoir Depth (km)	Lateral Length (km)	Injection Temperature (°C)	Flow Rate (kg·s^{-1})	Fluid	Simulator
1	CXA	200°C	2 km	0 km	20°C	20 kg·s^{-1}	Water	SBT/ COM
7	CXA	200°C	2 km	0 km	**10°C**	20 kg·s^{-1}	Water	SBT/ COM
8	CXA	200°C	2 km	0 km	**40°C**	20 kg·s^{-1}	Water	SBT/ COM

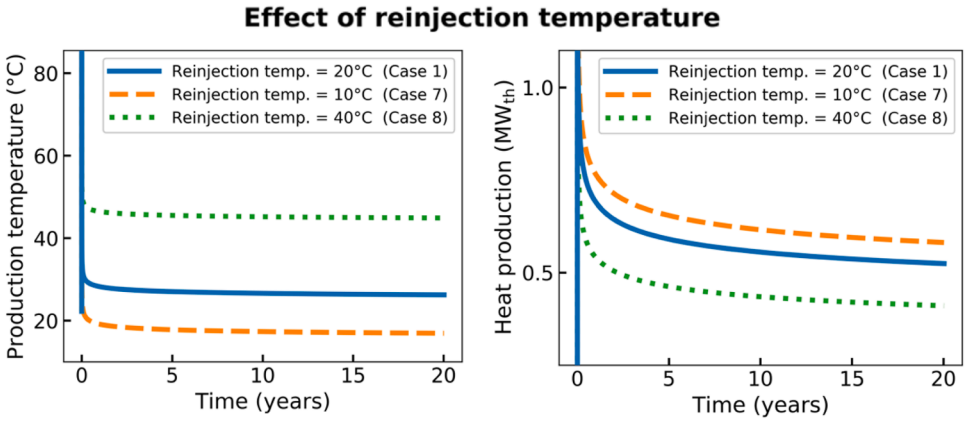

Fig. 5. Co-axial AGS simulation results for production temperature (°C) and produced heat (MW_{th}) for different injection temperature. Case 1 represents base case with injection temperature of 20°C. Case 7 and 8 consider injection temperature of 10°C and 40°C, respectively. Injection temperature has moderate impact on thermal performance with lower injection temperature resulting in lower production temperature but higher heat output. All cases assume CXA configuration, reservoir temperature of 150°C at 2 km depth, and water as heat transfer fluid with flow rate of 20 kg·s^{-1}.

Table 5
Co-axial AGS cases simulated to investigate impact of flow rate. Heat transfer within reservoir is through heat conduction only. Case 1 represents the co-axial AGS base case. The changes with respect to the base case are highlighted in bold. CXA = co-axial with injection in annulus; SBT = Slender Body Theory Model; COM = COMSOL Model.

Case No.	AGS Type	Reservoir Temperature (°C)	Reservoir Depth (km)	Lateral Length (km)	Injection Temperature (°C)	Flow Rate (kg·s^{-1})	Fluid	Simulator
1	CXA	200°C	2 km	0 km	20°C	20 kg·s^{-1}	Water	SBT/ COM
9	CXA	200°C	2 km	0 km	20°C	**10 kg·s^{-1}**	Water	SBT/ COM
10	CXA	200°C	2 km	0 km	20°C	**40 kg·s^{-1}**	Water	SBT/ COM

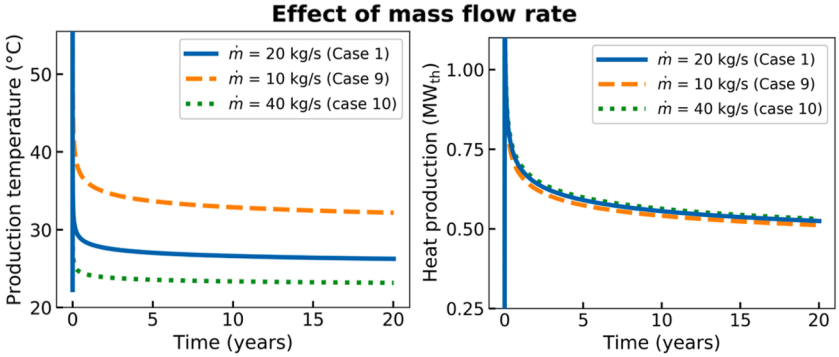

Fig. 6. Co-axial AGS simulation results for production temperature (°C) and produced heat (MW_{th}) for different flow rates. Case 1 represents base case with flow rate of 20 kg·s^{-1}. Cases 9 and 10 consider flow rate of 10 and 40 kg·s^{-1}, respectively. Operating at 10 kg·s^{-1} results in a higher production temperature and slightly lower heat production. At very low flow rates (~1 kg·s^{-1}), long-term production temperatures reach over 100°C, but heat production drops by more than 50%. All cases assume CXA configuration, reservoir temperature of 150°C at 2 km depth, and water as heat transfer fluid with injection temperature of 20°C.

relationship between injection temperature and heat production is approximately linear: a decrease in injection temperature results in a linear increase in heat production. Injection temperatures are dependent on the surface application. For example, electricity generation typically results in relatively high injection temperatures while heat pumps can achieve relatively low injection temperatures.

4.2.1.4. Impact of flow rate in co-axial systems. To assess the impact of mass flow rate, we again start with the co-axial base case (Case 1) but evaluate the effect of using a fluid rate of 10 and 40 kg·s^{-1} rather than 20 kg·s^{-1} (Table 5). Amongst the model results, a lower flow rate (Case 7) results in a higher production temperature but slightly lower heat output (Fig. 6). Keeping everything else constant, varying the flow rate allows to reach the target temperature as required for a certain surface

Table 6
Co-axial AGS cases simulated to investigate impact of utilizing sCO_2 as heat transfer fluid instead of water. Heat transfer within the reservoir is through heat conduction only. Case 8 represents the co-axial AGS base case but with 40°C injection temperature. CXA = co-axial with injection in annulus; SBT = Slender Body Theory Model; COM = COMSOL Model.

Case No.	AGS Type	Reservoir Temperature (°C)	Reservoir Depth (km)	Lateral Length (km)	Injection Temperature (°C)	Flow Rate ($kg{\cdot}s^{-1}$)	Fluid	Simulator
8	CXA	200°C	2 km	0 km	40°C	20 $kg{\cdot}s^{-1}$	Water	SBT/ COM
11	CXA	200°C	2 km	0 km	40°C	20 $kg{\cdot}s^{-1}$	**sCO_2**	SBT

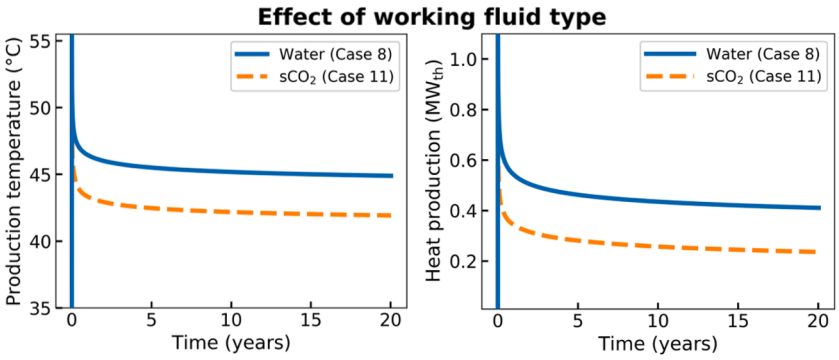

Fig. 7. Co-axial AGS simulation results for production temperature (°C) and produced enthalpy (MW_{th}) when using sCO_2 (Case 11) in comparison with the base case with 40°C injection temperature (Case 8). With all other conditions identical, utilizing sCO_2 instead of water results in 40% lower enthalpy gain. However, no pumping power is required with sCO2 as heat transfer fluid (Case 11), while, when utilizing water (Case 8), average pumping power is 9.5 kW_e. All cases assume CXA configuration, reservoir temperature of 150°C at 2 km depth, fluid flow rate of 20 $kg{\cdot}s^{-1}$ and fluid injection temperature of 20°C.

Table 7
Co-axial AGS cases simulated to investigate impact of injection in the center pipe rather than the annulus. Heat transfer within reservoir is through heat conduction only. Case 1 represents the co-axial AGS base case. The changes with respect to the base case are highlighted in bold. CXA = co-axial with injection in annulus; CXC = co-axial with injection in center pipe; SBT = Slender Body Theory Model; COM = COMSOL Model.

Case No.	AGS Type	Reservoir Temperature (°C)	Reservoir Depth (km)	Lateral Length (km)	Injection Temperature (°C)	Flow Rate ($kg{\cdot}s^{-1}$)	Fluid	Simulator
1	CXA	200°C	2 km	0 km	20°C	20 $kg{\cdot}s^{-1}$	Water	SBT/ COM
12	**CXC**	200°C	2 km	0 km	20°C	20 $kg{\cdot}s^{-1}$	Water	SBT/ COM

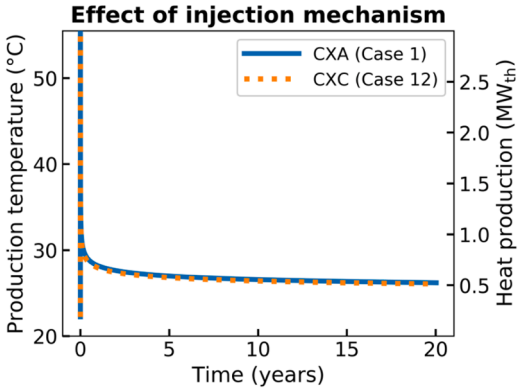

Fig. 8. Co-axial AGS simulation results for production temperature (°C) and produced heat (MW_{th}) for injection in center pipe (CXC) vs. injection in the annulus (CXA), which is the base case (Case 1). The impact is negligible with a slightly higher performance of the CXA configuration. All cases assume reservoir temperature of 150°C at 2 km depth, and water as heat transfer fluid with flow rate of 20 $kg{\cdot}s^{-1}$ and injection temperature of 20°C.

application. However, operating at very low flow rates also results in low levels of heat production. For example, additional SBT simulations show that operating at 1 $kg{\cdot}s^{-1}$ results in average production temperatures of around 100°C, but average heat production of only 0.23 MW_{th}. In comparison, the base case (Case 1; flow rate of 20 $kg{\cdot}s^{-1}$) results in average production temperatures of 27°C but average heat production of 0.57 MW_{th}.

4.2.1.5. Impact of heat transfer fluid type in co-axial systems. Case 11 (Table 6) uses sCO_2 instead of water as heat transfer working fluid for the co-axial configuration, resulting in average production temperature of 42.3°C and average heat production of 0.27 MW_{th} (Fig. 7). The injection temperature and pressure are set at 40°C and 10^7 Pa, respectively, to ensure CO_2 remains in the supercritical phase. In comparison, the equivalent case with water (Case 8) results in average production temperature of 45.3°C and average heat production of 0.45 MW_{th}. Hence, keeping everything else the same, utilizing sCO_2 instead of water results in 40% lower enthalpy gain. However, due to the thermosiphon effect, no pumping power was required when utilizing sCO_2 (Case 11) while the average pumping power with water (Case 8) is 9.5 kW_e. Potential for electricity production with sCO_2 is investigated in Section 4.4.

4.2.1.6. Impact of injection in annulus (CXA) vs. in center pipe (CXC). We now consider design choices in co-axial systems and evaluate whether thermal performance is impacted by choosing to drive heat exchange with injection in the center pipe (CXC) rather than in the annulus (CXA) as in our other co-axial simulations (Table 7). For the set of reservoir and operating conditions used in the co-axial base case (Case 1), we find that there is very little difference between CXA versus CXC — similar to the conclusions drawn by Holmberg et al. (2016) —, with injection in the annulus (CXA) performing just slightly better than injection in the center pipe (Fig. 8). However, we note that it is possible that this finding may not apply for other geometries or reservoir and operating conditions (Fox et al., 2016).

4.2.1.7. Impact of horizontal extension in co-axial systems. We now consider the influence of including a horizontal extension at the base of a

Table 8
Co-axial AGS cases simulated to investigate impact of a horizontal extension. Heat transfer within reservoir is through heat conduction only. Case 1 represents the co-axial AGS base case. The changes with respect to the base case are highlighted in bold. CXA = co-axial with injection in annulus; SBT = Slender Body Theory Model; COM = COMSOL Model.

Case No.	AGS Type	Reservoir Temperature (°C)	Reservoir Depth (km)	Lateral Length (km)	Injection Temperature (°C)	Flow Rate (kg·s^{-1})	Fluid	Simulator
1	CXA	200°C	2 km	0 km	20°C	20 kg·s^{-1}	Water	SBT/ COM
13	CXA	200°C	2 km	**2 km**	20°C	20 kg·s^{-1}	Water	SBT

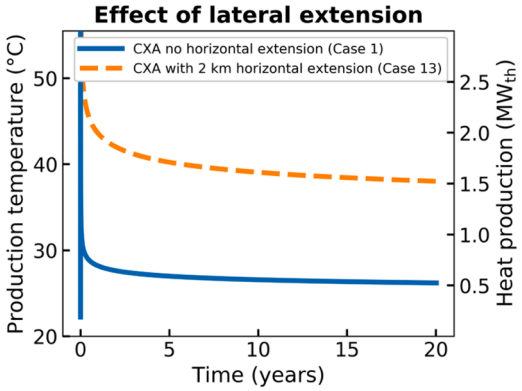

Fig. 9. Co-axial AGS simulation results for production temperature (°C) and produced heat (MW_{th}) when adding a 2 km long horizontal extension (Case 13) in comparison with the base case (Case 1). Increasing the subsurface heat exchanger length (and area) significantly increases the production temperature and heat output. All cases assume CXA configuration, reservoir temperature of 150°C at 2 km depth, and water as heat transfer fluid with flow rate of 20 kg·s^{-1} and injection temperature of 20°C.

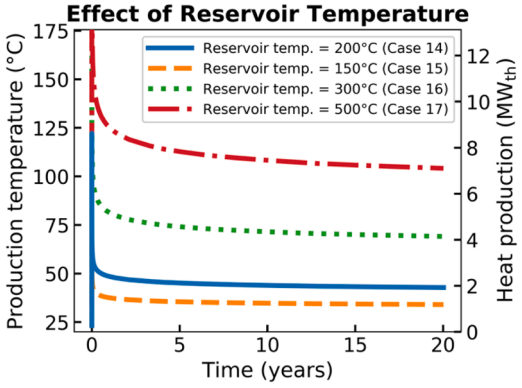

Fig. 10. U-loop AGS simulation results for production temperature (°C) and produced heat (MW_{th}) for different reservoir temperatures. Case 14 represents base case with reservoir temperature of 150°C at 2 km depth. Case 14 yields average heat production on the order of 2 MW_{th} with average production temperature of 45°C (25°C above the injection temperature). Cases 15 through 17 consider different reservoir temperatures. Case 17 with 500°C reservoir temperature at 2 km depth results in about 7.7 MW_{th} of average heat production. All cases assume U2-loop configuration, reservoir at 2 km depth, lateral length of 2 km, and water as heat transfer fluid with flow rate of 20 kg·s^{-1} and injection temperature of 20°C.

co-axial system. This type of design has been proposed as a way to increase the heat exchange area where formation temperatures are greatest. Comparing to the base case (Case 1), Case 13 simulates the effects of including a 2 km horizontal extension at 2 km depth (Table 8). The results (Fig. 9) illustrate that the horizontal extension increases the average production temperature from 27 to 40°C, and average heat production from ~0.6 MW_{th} to ~1.7 MW_{th}. Increasing the heat exchanger length within the reservoir significantly increases the surface area and boosts the system thermal performance.

4.2.2. U-loop AGS thermal performance in conduction-only reservoirs

Our results above describe the performance characteristics for various co-axial system scenarios and illustrate the potential impact horizontal laterals can have in increasing heat exchange and thermal performance. U-Loop AGS utilize an alternative closed-loop design that seek to take advantage of heat exchange through laterals with unidirectional flow between separate injection and production wellheads connected underground with various numbers of laterals.

4.2.2.1. Base Case and Impact of reservoir temperature in U-loop systems.

As a base case U-loop AGS design scenario (Case 14), we consider a system with two horizontal laterals of 2 km length at 2 km depth, 150°C reservoir temperature, and with water injected at 20°C and 20 kg·s^{-1}. The solid blue curve in Fig. 10 reveals the results, with average production temperature of ~45°C and average heat production of 2.1 MW_{th} (Fig. 10). Despite a lower reservoir temperature, these results show much greater thermal performance than the co-axial base case (Case 1) or the co-axial system with a 2 km horizontal extension (Case 13). Having two long laterals within the highest temperature region of the subsurface has a clear influence on the results. Similar to our analysis for the co-axial systems, we now explore in this and the following sections the influence of reservoir, operational, and design considerations on the thermal performance of U-loop systems.

Starting with the U-loop base case at 150°C reservoir temperature (Case 14), we consider three additional cases at a reservoir temperature of 100°C, 300°C and 500°C (Table 9). The relationship between reservoir temperature and thermal output (production temperature and heat production) is linear. Fig. 10 shows the average production temperature for a reservoir temperature of 100, 300 and 500°C is 35.2, 73.2 and 111.2°C, respectively. The corresponding average heat production is 1.3, 4.5 and 7.7 MW_{th}, respectively. The low-temperature scenario of 100°C at 2 km depth (Case 15), corresponds to a geothermal gradient of 40°C·km^{-1}, a typical gradient found in non-volcanic regions.

4.2.2.2. Impact of reservoir depth in U-loop systems.

We now consider the scenarios with the base case reservoir temperature (150°C) occurring at depths of 3 km (Case 18) and 4 km (Case 19) (see Table 10). Fig. 11 reveals an approximate linear increase of thermal output with depth. With 150°C at 3 km depth, the average heat production increases to 2.33 MW_{th}; with 150°C at 4 km depth, the average heat production is 2.57 MW_{th}. Larger depths result in an increase in heat exchange area and thermal output, but also causes the drilling costs to increase (see Section 4.5).

4.2.2.3. Impact of lateral length in U-loop systems.

We now simulate one case with horizontal lateral length of 4 km (Case 20) instead of the base case length of 2 km (Case 14) (see Table 11) to investigate impact of later length on U-loop thermal performance. Fig. 12 shows that the average production temperature increases to 57.8°C and the average heat production to 3.2 MW_{th}. Extending the heat exchanger length within the hottest zone of the reservoir significantly impacts the thermal performance. However, increasing the lateral length also increases the drilling cost (see Section 4.5).

Table 9
U-loop AGS cases simulated to investigate impact of reservoir temperature, depth and length of horizontal lateral. Heat transfer within the reservoir is through heat conduction only. Case 14 represents the U-loop AGS base case. U2 = U-loop with two horizontal laterals; SBT = Slender Body Theory Model

Case No.	AGS Type	Reservoir Temperature (°C)	Reservoir Depth (km)	Lateral Length (km)	Injection Temperature (°C)	Flow Rate (kg·s^{-1})	Fluid	Simulator
14	U2	150°C	2 km	2 km	20°C	20 kg·s^{-1}	Water	SBT
15	U2	**100°C**	2 km	2 km	20°C	20 kg·s^{-1}	Water	SBT
16	U2	**300°C**	2 km	2 km	20°C	20 kg·s^{-1}	Water	SBT
17	U2	**500°C**	2 km	2 km	20°C	20 kg·s^{-1}	Water	SBT

Table 10
U-loop AGS cases simulated to investigate impact of reservoir depth. Heat transfer within the reservoir is through heat conduction only. Case 14 represents the U-loop AGS base case. U2 = U-loop with two horizontal laterals; SBT = Slender Body Theory Model

Case No.	AGS Type	Reservoir Temperature (°C)	Reservoir Depth (km)	Lateral Length (km)	Injection Temperature (°C)	Flow Rate (kg·s^{-1})	Fluid	Simulator
14	U2	150°C	2 km	2 km	20°C	20 kg·s^{-1}	Water	SBT
18	U2	150°C	**3 km**	2 km	20°C	20 kg·s^{-1}	Water	SBT
19	U2	150°C	**4 km**	2 km	20°C	20 kg·s^{-1}	Water	SBT

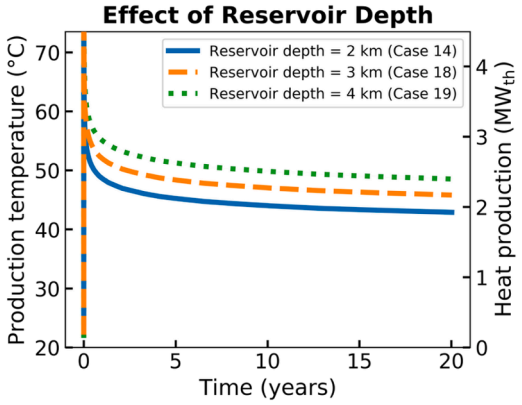

Fig. 11. U-loop AGS simulation results for production temperature (°C) and produced heat (MW_{th}) for different reservoir depths. Case 14 represents base case with reservoir temperature of 150°C at 2 km depth. Deeper reservoir depths result in a small increase in thermal output. All cases assume U2-loop configuration, lateral length of 2 km, reservoir of 150°C, and water as heat transfer fluid with flow rate of 20 kg·s^{-1} and injection temperature of 20°C.

4.2.2.4. Impact of fluid injection temperature in U-loop systems. Similar to the co-axial cases, we consider the influence of injection temperature by comparing our U-loop base case (Case 14) to cases in which the injection temperatures is 10 and 40°C rather than 20°C (Table 12; Fig. 13). The lower injection temperature of 10°C (Case 21) results in a lower average production temperature of ~37°C, but has a slightly larger average temperature gain and heat production of ~27°C and ~2.3 MW_{th}, respectively. The 40°C injection temperature case (Case 22) results in average heat production of ~1.6 MW_{th}. Similar as with the co-axial system, a lower injection temperature results in larger heat production. However, the injection temperature is a function of the surface application. Low injection temperatures may only be achieved when coupled with heat pumps.

4.2.2.5. Impact of mass flow rate in U-loop systems. To assess the influence of mass flow rate, we consider models similar to Case 14 (base case) but with flow rate of 10 and 40 kg·s^{-1} instead of 20 kg·s^{-1} (Table 13). Compared to the base case, the lower flow rate of 10 kg·s^{-1} (Case 23) results in higher average production temperature of ~63°C, but has poorer average heat production of ~1.8 MW_{th} (Fig. 14). The higher flow rate of 40 kg·s^{-1} (Case 24) results in lower production temperatures but slightly higher heat production than the base case at ~2.2 MW_{th}. Similar as with co-axial systems, the flow rate can be modified to target a certain temperature as required by the surface application. A very low flow rate results in much larger production temperatures but also significantly lowers the heat production. For example, circulating water at 2.5 kg·s^{-1} results in an average production temperature of ~100°C but average heat production of only ~0.84 MW_{th}.

4.2.2.6. Impact of fluid type in U-loop systems. Similar to Section 4.2.1.5 in which we investigate the influence of injection fluid type for co-axial systems, we also compare cases with either sCO_2 or water as heat transfer fluid for U-loop configurations (Table 14). For these cases, injection temperature and pressure are held at 40°C and 10^7 Pa,

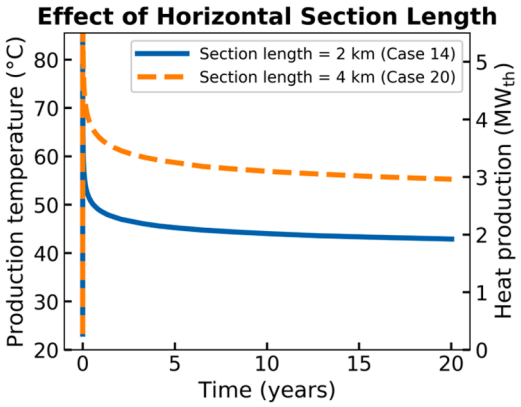

Fig. 12. U-loop AGS simulation results for production temperature (°C) and produced heat (MW_{th}) for different lateral lengths. Doubling the lateral length from 2 km to 4 km increasing the average heat production from 2.1 to 3.2 MW_{th}. All cases assume U2-loop configuration, reservoir of 150°C at 2 km depth, and water as heat transfer fluid with flow rate of 20 kg·s^{-1} and injection temperature of 20°C.

Table 11
U-loop AGS cases simulated to investigate impact of horizontal lateral length. Heat transfer within the reservoir is through heat conduction only. Case 14 represents the U-loop AGS base case. U2 = U-loop with two horizontal laterals; SBT = Slender Body Theory Model

Case No.	AGS Type	Reservoir Temperature (°C)	Reservoir Depth (km)	Lateral Length (km)	Injection Temperature (°C)	Flow Rate (kg·s^{-1})	Fluid	Simulator
14	U2	150°C	2 km	2 km	20°C	20 kg·s^{-1}	Water	SBT
20	U2	150°C	2 km	**4 km**	20°C	20 kg·s^{-1}	Water	SBT

Table 12
U-loop AGS cases simulated to investigate impact of fluid injection temperature. Heat transfer within the reservoir is through heat conduction only. Case 14 represents the U-loop AGS base case. U2 = U-loop with two horizontal laterals; SBT = Slender Body Theory Model

Case No.	AGS Type	Reservoir Temperature (°C)	Reservoir Depth (km)	Lateral Length (km)	Injection Temperature (°C)	Flow Rate ($kg{\cdot}s^{-1}$)	Fluid	Simulator
14	U2	150°C	2 km	2 km	20°C	20 $kg{\cdot}s^{-1}$	Water	SBT
21	U2	150°C	2 km	2 km	**10°C**	20 $kg{\cdot}s^{-1}$	Water	SBT
22	U2	150°C	2 km	2 km	**40°C**	20 $kg{\cdot}s^{-1}$	Water	SBT

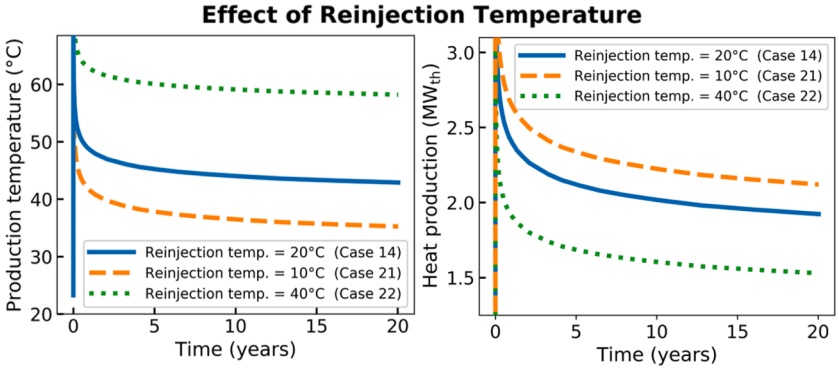

Fig. 13. U-loop AGS simulation results for production temperature (°C) and produced heat (MW_{th}) for different fluid injection temperature. Case 14 represents base case with injection temperature of 20°C. Cases 21 and 22 consider injection temperature of 10°C and 40°C, respectively. A lower injection temperature increases the temperature gain and heat production. All cases assume U2-loop configuration with lateral length of 2 km, reservoir of 150°C at 2 km depth, and water as heat transfer fluid with flow rate of 20 $kg{\cdot}s^{-1}$.

Table 13
U-loop AGS cases simulated to investigate impact of fluid flow rate. Heat transfer within the reservoir is through heat conduction only. Case 14 represents the U-loop AGS base case. U2 = U-loop with two horizontal laterals; SBT = Slender Body Theory Model

Case No.	AGS Type	Reservoir Temperature (°C)	Reservoir Depth (km)	Lateral Length (km)	Injection Temperature (°C)	Flow Rate ($kg{\cdot}s^{-1}$)	Fluid	Simulator
14	U2	150°C	2 km	2 km	20°C	20 $kg{\cdot}s^{-1}$	Water	SBT
23	U2	150°C	2 km	2 km	20°C	**10 $kg{\cdot}s^{-1}$**	Water	SBT
24	U2	150°C	2 km	2 km	20°C	**40 $kg{\cdot}s^{-1}$**	Water	SBT

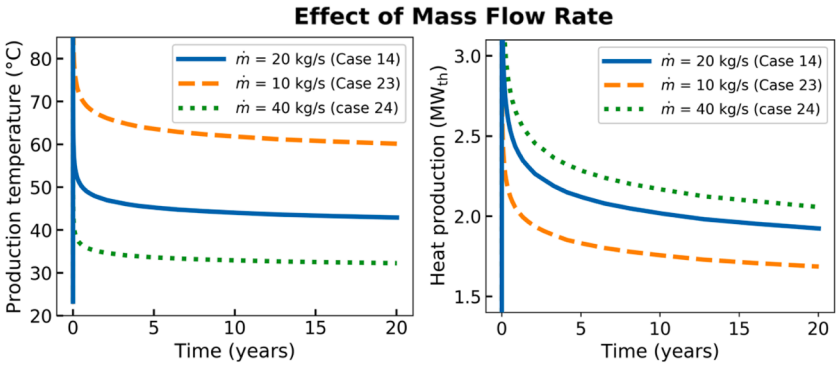

Fig. 14. U-loop AGS simulation results for production temperature (°C) and produced heat (MW_{th}) for different fluid flow rates. Case 14 represents base case with flow rate of 20 $kg{\cdot}s^{-1}$. Cases 23 and 24 consider flow rate of 10 $kg{\cdot}s^{-1}$ and 40 $kg{\cdot}s^{-1}$, respectively. Increasing the flow rate decreases the production temperature but slightly increases the heat production. All cases assume U2-loop configuration with lateral length of 2 km, reservoir of 150°C at 2 km depth, and water as heat transfer fluid with injection temperature of 20°C.

Table 14
U-loop AGS cases simulated to investigate impact of fluid type. Heat transfer within the reservoir is through heat conduction only. Case 22 represents the U-loop AGS base case with water but with 40°C injection temperature. U2 = U-loop with two horizontal laterals; SBT = Slender Body Theory Model

Case No.	AGS Type	Reservoir Temperature (°C)	Reservoir Depth (km)	Lateral Length (km)	Injection Temperature (°C)	Flow Rate ($kg{\cdot}s^{-1}$)	Fluid	Simulator
22	U2	150°C	2 km	2 km	40°C	20 $kg{\cdot}s^{-1}$	Water	SBT
25	U2	150°C	2 km	2 km	40°C	20 $kg{\cdot}s^{-1}$	**sCO_2**	SBT

respectively, to ensure CO_2 remains in the supercritical phase. Whereas the case with injection of 40°C water (Case 22) results in average heat production of ~1.6 MW_{th}, the average enthalpy gain for sCO_2 (Case 25) is only ~1 MW_{th} (Fig. 15). However, Case 22 (water) requires an average pumping power of 2 kW_e while Case 25 (sCO_2) does not require pumping power because of the strong the thermosiphon effect. In fact, due to the large gain in pressure between injection and production with sCO_2, about 90 kWe of electricity could be produced when directly coupled to a turbine (see also Section 4.4). The results indicate that if AGS is used for heat production, water appears the preferred heat transfer fluid. In case of electricity generation, the results are more nuanced (see Section 4.4).

4.2.2.7. Impact of number of laterals. Because thermal performance is expected to improve with greater heat exchange area within the reservoir, we evaluate the influence of increasing the number of horizontal

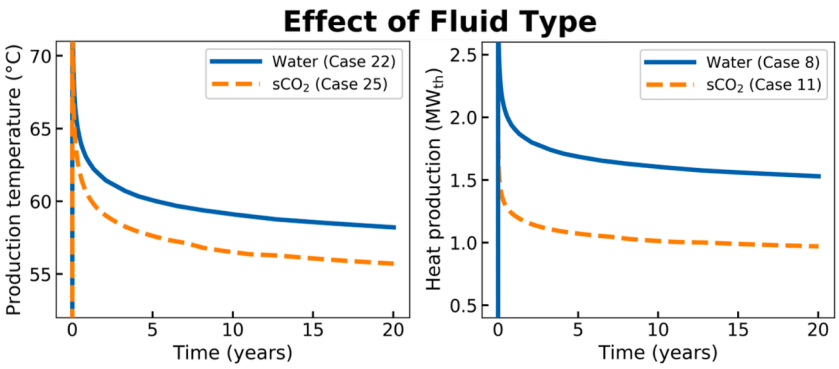

Fig. 15. U-loop AGS simulation results for production temperature (°C) and produced heat (MW_{th}) for sCO_2 versus water as heat transfer fluid. Case 22 represents base case with two laterals but with 40°C injection temperature. Case 25 is identical to Case 22 but with sCO_2 instead of water. Utilizing sCO_2 instead of water results in a slight decrease in production temperature and a significant drop in enthalpy output of about 40%. All cases assume U2-loop configuration with lateral length of 2 km, reservoir of 150°C at 2 km depth, fluid flow rate of 20 $kg{\cdot}s^{-1}$, and fluid injection temperature of 20°C.

Table 15
U-loop AGS cases simulated to investigate impact of number of horizontal laterals. Heat transfer within the reservoir is through heat conduction only. Case 14 represents the U-loop AGS base case. U2 = U-loop with two horizontal laterals; U5 = U-loop with five horizontal laterals; U13 = U-loop with thirteen number of laterals; SBT = Slender Body Theory Model

Case No.	AGS Type	Reservoir Temperature (°C)	Reservoir Depth (km)	Lateral Length (km)	Injection Temperature (°C)	Flow Rate ($kg{\cdot}s^{-1}$)	Fluid	Simulator
14	U2	150°C	2 km	2 km	20°C	20 $kg{\cdot}s^{-1}$	Water	SBT
26	**U5**	150°C	2 km	2 km	20°C	20 $kg{\cdot}s^{-1}$	Water	SBT
27	**U13**	150°C	2 km	2 km	20°C	20 $kg{\cdot}s^{-1}$	Water	SBT

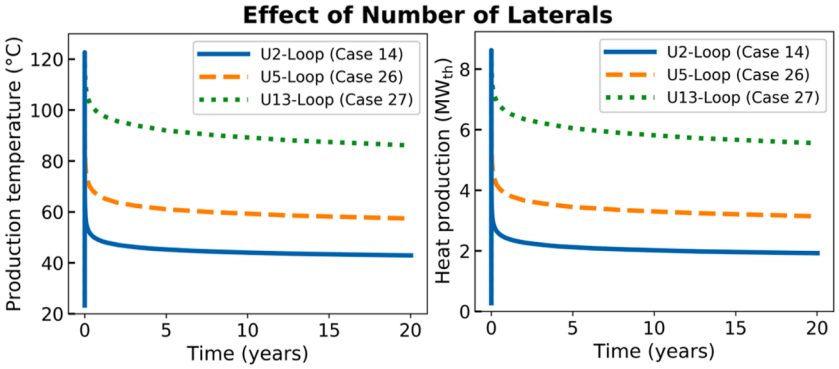

Fig. 16. U-loop AGS simulation results for production temperature (°C) and produced heat (MW_{th}) for different number of horizontal laterals. Case 14 represents base case with two laterals. Cases 26 and 27 consider five and thirteen laterals, respectively. Increasing the number of laterals significantly increases the production temperature and heat production. All cases assume U-loop configuration with lateral length of 2 km, reservoir of 150°C at 2 km depth, and water as heat transfer fluid with flow rate of 20 $kg{\cdot}s^{-1}$ and injection temperature of 20°C.

Table 16
Co-axial AGS cases simulated with natural convection in the reservoir. Different cases consider different values for reservoir permeability. CXC = co-axial with injection in center pipe; SBT = Slender-Body Theory Model; COM = COMSOL Model

Case No.	AGS Type	Reservoir Temperature (°C)	Reservoir Depth (km)	Lateral Length (km)	Injection Temperature (°C)	Flow Rate ($kg{\cdot}s^{-1}$)	Fluid	Reservoir Permeability (m^2)	Simulator
12	CXC	200°C	2 km	0 km	20°C	20 $kg{\cdot}s^{-1}$	Water	0 (conduction-only)	SBT/ COM
28	CXC	200°C	2 km	0 km	20°C	20 $kg{\cdot}s^{-1}$	Water	$\mathbf{10^{-18}\ m^2}$	COM
29	CXC	200°C	2 km	0 km	20°C	20 $kg{\cdot}s^{-1}$	Water	$\mathbf{10^{-15}\ m^2}$	COM

laterals (Cases 26 and 27; Table 15) compared to our base case (Case 14). Fig. 16 illustrates that including additional laterals results in larger production temperature and heat output. A U-loop with five laterals (Case 26) results in an average production temperature of ~60°C and average heat production of ~3.1 MW_{th}. A U-loop with thirteen laterals (Case 27) increases the average production temperature to ~90°C and average heat production to ~5.9 MW_{th}. Thermal performance increases because adding laterals increases the surface area for heat transfer between the fluid and the rock. However, adding laterals also significantly increases capital costs (Section 4.5). Further, connecting a large number of horizontal laterals to the same point at the injection and production well may introduce technical challenges for drilling and completing such configuration. Branching across different points may be required when developing a large number of laterals.

4.3. AGS thermal performance with convection in reservoir

So far, all of our scenarios assume conductive heat transfer through the rock formation outside of the closed-loop pipe. As shown in Sections 4.1 and 4.2, this limits heat exchange for both co-axial and U-loop and results in rapid decline in thermal output. In these conduction-dominated systems, heat is rapidly extracted from the formation directly surrounding the heat exchanger but is unable to be replenished quickly by thermal diffusion alone. Some AGS designs seek to overcome this limitation by relying on geologic conditions that allow for convection within the reservoir. Here, we expand on our analysis to assess the potential influence natural or forced convection within the reservoir has on AGS thermal performance.

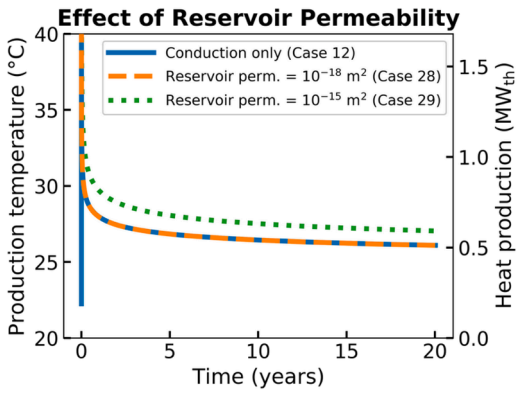

Fig. 17. Simulation results of co-axial AGS with natural convection in the reservoir versus heat conduction-only. A typical reservoir permeability of 10^{-15} m^2 (~1 mD) results in 20% increase in heat production with respect to the heat conduction-only scenario. All cases assume a CXC configuration with reservoir temperature of 200°C at 2 km depth, and water as heat transfer fluid with flow rate of 20 $kg{\cdot}s^{-1}$ and injection temperature of 20°C.

4.3.1. AGS thermal performance with natural convection in reservoir

To investigate the impact of natural convection within the reservoir on the thermal performance of co-axial AGS we consider two cases (Cases 28 and 29) with different reservoir permeability (Table 16). These simulations utilize COMSOL which solves for the fluid flow and heat transport in both the pipe and formation. Due to convergence issues with the CXA configuration, we consider a CXC scenario (injection in the center pipe and return flow in the annulus). Case 29 assumes a permeability of 10^{-15} m^2 (~1 mD), which represents a typical in-situ permeability in the continental crust at 2 km depth (Ingebritsen and Manning, 2010). Simulation results (Fig. 17) indicate that with a permeability of 10^{-15} m^2, (Case 29), average thermal output increases by about 20% in comparison with the conduction-only scenario. The thermal output for Case 28 with very low permeability of 10^{-18} m^2 overlaps with the conduction-only case (Case 12). Even at moderate depths of 2 to 4 km, a low permeability of 10^{-18} m^2 is not uncommon, e.g., in granite or shale formations. This suggests that the conduction-only cases that we consider in Section 4.2 are representative in many scenarios.

Similarly, we examine the influence of natural reservoir convection for U-loop systems. We consider two cases (Cases 30 and 31) with different reservoir permeability to investigate impact of natural convection on thermal performance (Table 17). We assume a U-loop geometry with only one lateral and simulate performance with COMSOL. To save on computational time, only the horizontal section is simulated, corresponding to a scenario with a perfectly insulated injection and production well. The thermal output of the low permeability case (Case 26) with permeability of 10^{-18} m^2 overlaps with the result for a conduction-only case. The scenario with higher permeability of 10^{-15} m^2 (~1 mD; Case 31) results in an increase in the heat production by about 4% compared to the conduction-dominated case (Fig. 17). Due to numerical convergence issues, we did not run simulations for higher permeabilities. Oldenburg et al. (2016) report that natural convection can cause a 100% increase in U-loop heat production in case a very high permeable zone (permeability of 10^{-10} m^2 or 100 D) directly surrounds the heat exchanger. However, the results by Ingebritsen and Manning (2010) suggest that at depths of 2 to 4 km, in-situ reservoir permeability (i.e., matrix permeability and not fracture permeability) much higher than 10^{-15} m^2 is not commonly encountered. The results from our simulations (Cases 28 through 31) and those by Oldenburg et al. (2016) suggest that very high in-situ reservoir permeability is required to obtain significant improvements in heat production with AGS due to natural convection. For typical reservoir permeabilities of 10^{-15} m^2 at the depths we consider (2 to 4 km), increase in AGS thermal output due to natural convection is limited.

4.3.2. AGS thermal performance with forced convection in reservoir

Three cases (Cases 32 to 34) for U-loop AGS with one lateral are conducted with forced uniform convection ("background flow") in the reservoir with different values for Darcy velocity (Table 18). Simulations were conducted with the SBT model. Results indicate that Darcy velocities of at least 10^{-6} $m{\cdot}s^{-1}$ are required to obtain a considerable

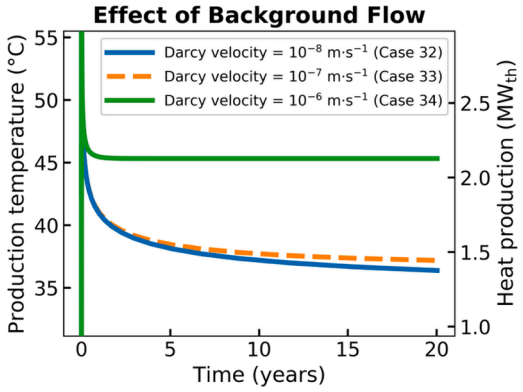

Fig. 19. Simulation results of U-loop AGS with forced convection in the reservoir for different values of Darcy velocity. Darcy velocities of 10^{-7} $m{\cdot}s^{-1}$ or lower had limited impact on thermal performance. A Darcy velocity of 10^{-6} $m{\cdot}s^{-1}$ resulted in significant increase in thermal output. All cases assume a U1-loop configuration with lateral length of 2 km, reservoir temperature of 150°C at 2 km depth, and water as heat transfer fluid with flow rate of 20 $kg{\cdot}s^{-1}$ and injection temperature of 20°C.

Table 17
U-loop AGS cases simulated with natural convection in the reservoir with different values for reservoir permeability. U1 = U-loop with one lateral; COM = COMSOL Model

Case No.	AGS Type	Reservoir Temperature (°C)	Reservoir Depth (km)	Lateral Length (km)	Injection Temperature (°C)	Flow Rate ($kg{\cdot}s^{-1}$)	Fluid	Reservoir Permeability (m^2)	Simulator
30	U1	120°C	2 km	2 km	20°C	20 $kg{\cdot}s^{-1}$	Water	**10^{-18} m^2**	COM
31	U1	120°C	2 km	2 km	20°C	20 $kg{\cdot}s^{-1}$	Water	**10^{-15} m^2**	COM

Table 18
U-loop AGS cases simulated with forced convection in the reservoir with different values of Darcy Velocity. All cases consider a U-loop design with one lateral. U1 = U-loop with one lateral; SBT = Slender Body Theory Model.

Case No.	AGS Type	Reservoir Temperature (°C)	Reservoir Depth (km)	Lateral Length (km)	Injection Temperature (°C)	Flow Rate ($kg{\cdot}s^{-1}$)	Fluid	Darcy Velocity ($m{\cdot}s^{-1}$)	Simulator
32	U1	150°C	2 km	2 km	20°C	20 $kg{\cdot}s^{-1}$	Water	**10^{-8} $m{\cdot}s^{-1}$**	SBT
33	U1	150°C	2 km	2 km	20°C	20 $kg{\cdot}s^{-1}$	Water	**10^{-7} $m{\cdot}s^{-1}$**	SBT
34	U1	150°C	2 km	2 km	20°C	20 $kg{\cdot}s^{-1}$	Water	**10^{-6} $m{\cdot}s^{-1}$**	SBT

Table 19
List of AGS cases simulated for electricity generation. For each case, the flow rate was varied to maximize the electricity production. CXA = co-axial with injection in annulus; U2 = U-loop with two laterals; SBT = Slender Body Theory Model.

Case No.	AGS Type	Reservoir Temperature (°C)	Reservoir Depth (km)	Lateral Length (km)	Injection Temperature (°C)	Flow Rate ($kg{\cdot}s^{-1}$)	Fluid	Simulator
35	CXA	200°C	2 km	0 km	70°C	2.5 $kg{\cdot}s^{-1}$	Water	SBT
36	CXA	200°C	2 km	0 km	40°C	2.8 $kg{\cdot}s^{-1}$	sCO_2	SBT
37	CXA	500°C	2 km	0 km	80°C	2.0 $kg{\cdot}s^{-1}$	Water	SBT
38	U2	150°C	2 km	2 km	70°C	10 $kg{\cdot}s^{-1}$	Water	SBT
39	U2	150°C	2 km	2 km	40°C	15 $kg{\cdot}s^{-1}$	sCO_2	SBT
40	U2	500°C	2 km	2 km	80°C	11 $kg{\cdot}s^{-1}$	Water	SBT

impact on the thermal output (Fig. 19). These are relatively high Darcy velocities, which typically do not occur naturally in deep formations.

4.4. Performance of AGS for electricity production

We now consider co-axial and U-loop AGS for electricity production. We simulate six new cases (Table 9) to investigate the potential for electricity generation with the co-axial (Case 1) and U-loop (Case 14) base case for commonly encountered reservoir rock temperatures ranging from 150 to 200°C. We also include a co-axial and U-loop case at a much higher reservoir rock temperature of 500°C at an assumed 2 km depth (Cases 4 and 17, respectively). We consider both water and sCO_2 as reservoir fluids The cases considered in Sections 4.2 and 4.3 result in production temperatures on the order of 20 to 60°C, too low to produce electricity. Generally, production temperatures over 80°C are required to generate electricity with sufficiently high conversion efficiencies. Here, we lower the flow rate in each case (see Table 19) to maximize the electricity production. For water as heat transfer fluid, the injection temperature is increased to 70 to 80°C to represent more typical injection temperatures when producing electricity with an ORC power plant (Beckers, 2016). Produced electricity for these cases is estimated by calculating the produced exergy and multiplying by a temperature-dependent utilization efficiency for a subcritical ORC plant (Beckers, 2016). In Cases 36 and 39, the working fluid sCO_2 directly drives a turbine with an assumed isentropic turbine efficiency of 0.9.

For the co-axial base case scenario (200°C at 2 km depth), we find a maximum average electricity production of ~14 kW_e when using water as heat transfer fluid at 2.5 $kg{\cdot}s^{-1}$ (Case 35). The average production temperature in this case is ~93°C and, due to the strong thermosiphon effect, no pumping power is required. When utilizing sCO_2 instead of water, we find a maximum average electricity production of ~23 kW_e when circulating at 2.8 $kg{\cdot}s^{-1}$ (Case 36). For the high-temperature co-axial scenario (500°C at 2 km), we obtain a higher electricity output for water than for sCO_2. With water circulating at 2 $kg{\cdot}s^{-1}$ (Case 37), we find a maximum electricity production of ~133 kW_e, with an average production temperature of ~190°C and no pumping power required. When utilizing sCO_2 as working fluid, the maximum average electricity production is 104 kW_e at 6 $kg{\cdot}s^{-1}$.

For the base case U-loop scenario (150°C at 2 km depth with 2 laterals of 2 km length), the maximum average electricity production with water is ~51 kW_e when circulating at 10 $kg{\cdot}s^{-1}$ (Case 38). For this case, the average production temperature is 91°C and no pumping power is required. When utilizing sCO_2 instead of water, the electricity production increases up to ~92 kW_e at 15 $kg{\cdot}s^{-1}$ (Case 39). With a 500°C reservoir at 2 km depth (Case 40), we find a maximum electricity production of ~857 kW_e when circulating water at 15 $kg{\cdot}s^{-1}$. For this case, the average production temperature is 202°C and no pumping power is required. When utilizing sCO_2 instead of water with a 500°C reservoir, the maximum power output is only ~741 kW_e.

These results suggest that electricity generation with AGS is challenging. For the geometries considered (2 km reservoir depth and lateral length of 2 km for the U2 configuration), low flow rates are required to obtain sufficiently high production temperatures and conversion efficiencies. While the base case co-axial and U-loop scenarios (Cases 1 and 14) produce usable heat at ~0.6 and ~2.1 MW_{th}, respectively, we find a maximum electricity production for these scenarios at only ~23 and ~92 kW_e, respectively. In both the co-axial and U-loop base case, sCO_2 performed better than water for electricity generation, while at very high reservoir temperatures, water performed best for electricity production. Higher levels of electricity production can be obtained by increasing the borehole heat transfer area (e.g., with a larger number of laterals). However, considering AGS first for heat production over electricity generation appears preferable.

4.5. Capital and Levelized Cost of AGS for Heat and Electricity Production

Using our various case scenario results, we now perform a high-level economic assessment with GEOPHIRES (Beckers and McCabe, 2019) to estimate capital costs, LCOH, and LCOE for AGS. We conduct these calculations for Cases 1 through 27 (direct-use heat) and Cases 35 through 40 (electricity) in which heat transfer within the reservoir is conduction-only. We assume a utilization rate of 100% with a discount rate of 5% and a system lifetime of 20 years. In general, we assume generous cost and financial conditions. Drilling costs for vertical wells are estimated using the "intermediate 1" drilling cost curves developed by Lowry et al. (2017) for the *GeoVision* study DOE (2019)(DOE - U.S. Department of Energy 2019). These drilling cost figures assume a reduction of about 50% from the baseline cost correlations. No published drilling cost correlations are available for the horizontal laterals. Their drilling costs may be significantly lower than the costs for the vertical wells because they may be completed without casing or cement. In this analysis, we assume a range in drilling costs for the horizontal laterals at $200/m to $1,000/m. $1,000/m should be easily achievable with today's technology while $200/m may be an aggressive target for the future. We do not consider exploration costs and surface pipeline costs.

For the vertical co-axial cases without the lateral extension (Cases 1 through 12, and 35 to 37), we utilize the cost correlation function for vertical wells with large diameter, while for Case 13 (vertical co-axial with horizontal extension), we use the cost correlation for deviated wells with large diameter. For the U-loop configurations (Cases 14 through 27, and 38 to 40), we use the cost correlation for vertical wells with small diameter for the vertical injection and production well and $200-$1000/m for the horizontal laterals.

The cost for a pipe-in-pipe system with vacuum insulated tubing for the co-axial configurations is estimated at $0.5M for 2 km measured depth, $0.75M for 3 km measured depth, and $1M for 4 km measured depth. For the cases considering direct-use heating, we estimate the cost for surface equipment (i.e., surface heat exchanger, valves, sensors and control) at $200/$kW_{th}$. For electricity generation with an ORC, capital costs for the power plant are estimated at $10,000/$kW_e$ for the ~14 kW_e system (Case 35), $5,000/kW for the 0.1 MW_e systems (Cases 37 and 38), and $3,000/$kW_e$ (Beckers and McCabe, 2019) for the ~0.9 MWe system (Case 40). For electricity production with sCO_2, capital costs for surface equipment are estimated at $4,000/$kW_e$ for a 23 kW_e sized system (Case 36) and $2,000/$kW_e$ for the 90 kW_e sized system (Case 39), based on cost numbers provided by Carlson et al. (2017). We assume that operation & maintenance costs are negligible for direct-use systems while they are set at 1% of the surface capital cost per year for electricity

Table 20
Estimates of average heat production (in GWh/year), capital costs (in $M) and levelized costs for heat (LCOH) (in $/MWh) for Cases 1 to 27 for direct-use heating (heat conduction-only in reservoir). Cost results for U-loop cases are presented for a horizontal lateral drilling cost of $1,000/m and $200/m.

Case No.	Case Description	Average Heat Production (GWh/year)	Capital Cost ($M)	Specific Capital Cost ($/kW$_{th}$)	LCOH ($/MWh)
1	CXA; 200°C at 2 km; 20 kg·s^{-1} water at 20°C	5.0	3.4	5,800	52.2
2	CXA; 150°C at 2 km; 20 kg·s^{-1} water at 20°C	3.6	3.3	8,000	71.6
3	CXA; 300°C at 2 km; 20 kg·s^{-1} water at 20°C	7.8	3.4	3,800	34.2
4	CXA; 500°C at 2 km; 20 kg·s^{-1} water at 20°C	13.5	3.6	2,300	20.7
5	CXA; 200°C at 3 km; 20 kg·s^{-1} water at 20°C	7.5	4.8	5,600	49.8
6	CXA; 200°C at 4 km; 20 kg·s^{-1} water at 20°C	9.8	6.0	5,300	47.6
7	CXA; 200°C at 2 km; 20 kg·s^{-1} water at 10°C	5.6	3.4	5,300	47.3
8	CXA; 200°C at 2 km; 20 kg·s^{-1} water at 40°C	4.0	3.3	7,400	66.2
9	CXA; 200°C at 2 km; 10 kg·s^{-1} water at 20°C	4.9	3.4	6,000	53.7
10	CXA; 200°C at 2 km; 40 kg·s^{-1} water at 20°C	5.1	3.4	5,800	51.5
11	CXA; 200°C at 2 km; 20 kg·s^{-1} sCO_2 at 40°C	2.4	3.3	12,200	108.3
12	CXC; 200°C at 2 km; 20 kg·s^{-1} water at 20°C	4.9	3.4	6,000	53.6
13	CXA with 2 km horizontal extension; 200°C at 2 km; 20 kg·s^{-1} water at 20°C	14.6	6.6	4,000	35.4
14	U2-Loop; 150°C at 2 km; 2 km lateral; 20 kg·s^{-1} water at 20°C	18.2	8.6 ($1,000/m) 5.4 ($200/m)	4,200 ($1,000/m) 2,600 ($200/m)	37.4 ($1,000/m) 23.5 ($200/m)
15	U2-Loop; 100°C at 2 km; 2 km lateral; 20 kg·s^{-1} water at 20°C	11.2	8.5 ($1,000/m) 5.3 ($200/m)	6,600 ($1,000/m) 4,100 ($200/m)	59.6 ($1,000/m) 37.1 ($200/m)
16	U2-Loop; 300°C at 2 km; 2 km lateral; 20 kg·s^{-1} water at 20°C	39.1	9.1 ($1,000/m) 5.9 ($200/m)	2,000 ($1,000/m) 1,300 ($200/m)	18.3 ($1,000/m) 11.9 ($200/m)
17	U2-Loop; 500°C at 2 km; 2 km lateral; 20 kg·s^{-1} water at 20°C	67.1	9.8 ($1,000/m) 6.6 ($200/m)	1,300 ($1,000/m) 900 ($200/m)	11.4 ($1,000/m) 7.7 ($200/m)
18	U2-Loop; 150°C at 3 km; 2 km lateral; 20 kg·s^{-1} water at 20°C	20.4	9.8 ($1,000/m) 6.6 ($200/m)	4,200 ($1,000/m) 2,800 ($200/m)	37.9 ($1,000/m) 25.5 ($200/m)
19	U2-Loop; 150°C at 4 km; 2 km lateral; 20 kg·s^{-1} water at 20°C	22.5	11.3 ($1,000/m) 8.1 ($200/m)	4,400 ($1,000/m) 3,100 ($200/m)	39.5 ($1,000/m) 28.3 ($200/m)
20	U2-Loop; 150°C at 2 km; 4 km lateral; 20 kg·s^{-1} water at 20°C	27.9	12.9 ($1,000/m) 6.5 ($200/m)	4,000 ($1,000/m) 2,000 ($200/m)	36.4 ($1,000/m) 18.3 ($200/m)
21	U2-Loop; 150°C at 2 km; 2 km lateral; 20 kg·s^{-1} water at 10°C	20.0	8.7 ($1,000/m) 5.5 ($200/m)	3,800 ($1,000/m) 2,400 ($200/m)	34.1 ($1,000/m) 21.5 ($200/m)
22	U2-Loop; 150°C at 2 km; 2 km lateral; 20 kg·s^{-1} water at 40°C	14.5	8.5 ($1,000/m) 5.3 ($200/m)	5,200 ($1,000/m) 3,200 ($200/m)	46.5 ($1,000/m) 29.1 ($200/m)
23	U2-Loop; 150°C at 2 km; 2 km lateral; 10 kg·s^{-1} water at 20°C	15.7	8.6 ($1,000/m) 5.4 ($200/m)	4,800 ($1,000/m) 3,000 ($200/m)	43.0 ($1,000/m) 27.0 ($200/m)
24	U2-Loop; 150°C at 2 km; 2 km lateral; 40 kg·s^{-1} water at 20°C	19.6	8.7 ($1,000/m) 5.5 ($200/m)	3,900 ($1,000/m) 2,400 ($200/m)	34.8 ($1,000/m) 21.9 ($200/m)
25	U2-Loop; 150°C at 2 km; 2 km lateral; 20 kg·s^{-1} sCO_2 at 40°C	9.2	8.4 ($1,000/m) 5.2 ($200/m)	8,100 ($1,000/m) 5,000 ($200/m)	72.3 ($1,000/m) 44.9 ($200/m)
26	U5-Loop; 150°C at 2 km; 2 km lateral; 20 kg·s^{-1} water at 20°C	29.6	14.9 ($1,000/m) 6.9 ($200/m)	4,400 ($1,000/m) 2,000 ($200/m)	39.7 ($1,000/m) 18.4 ($200/m)
27	U13-Loop; 150°C at 2 km; 2 km lateral; 20 kg·s^{-1} water at 20°C	51.8	31.4 ($1,000/m) 10.6 ($200/m)	5,300 ($1,000/m) 1,800 ($200/m)	47.9 ($1,000/m) 16.2 ($200/m)

Table 21
Estimates of average electricity production (in GWh/year), capital costs (in $M) and levelized costs for electricity (LCOE) (in $/MWh) for Cases 35 through 40 for electricity generation (with heat conduction-only in reservoir). Cost results for U-loop cases are presented for a horizontal lateral drilling cost of $1,000/m and $200/m.

Case No.	Case Description	Average Electricity Prod. (GWh/year)	Capital Cost ($M)	Specific Capital Cost ($/kW$_e$)	LCOE ($/MWh)
35	CXA; 200°C at 2 km; water	0.12	3.4	245,800	2,213
36	CXA; 200°C at 2 km; sCO_2	0.20	3.3	146,700	1,315
37	CXA; 500°C at 2 km; water	1.16	3.9	29,500	267
38	U2-Loop; 150°C at 2 km; 2 km lateral; water	0.45	8.5 ($1,000/m) 5.3 ($200/m)	166,700 ($1,000/m) 103,100 ($200/m)	1,501 ($1,000/m) 937 ($200/m)
39	U2-Loop; 150°C at 2 km; 2 km lateral; sCO_2	0.80	8.4 ($1,000/m) 5.2 ($200/m)	91,800 ($1,000/m) 56,800 ($200/m)	825 ($1,000/m) 512 ($200/m)
40	U2-Loop; 500°C at 2 km; 2 km lateral; water	7.51	10.8 ($1,000/m) 7.6 ($200/m)	12,600 ($1,000/m) 8,900 ($200/m)	116 ($1,000/m) $83/m ($200/m)

production.

Table 20 summarizes the results of our estimates of average annual heat production, capital costs, and LCOH for Cases 1 through 27. LCOH values range from $8/MWh to $108/MWh, with the co-axial base case (Case 1) LCOH at $52/MWh, and the U-loop base case (Case 14) at $37/MWh (with $1,000/m drilling cost for horizontal laterals). Specific capital cost estimates range from ~$900 to ~$12,000/kW$_{th}$. The co-axial base case capital cost estimate is $3.4M ($5,800/kW$_{th}$), and the U-loop base case capital cost is $8.6M ($4,200/kW$_{th}$). Results for average annual electricity production, capital costs, and LCOE for Cases 35 to 40 are presented in Table 21. LCOE values range from $83/MWh to $2,200/MWh. Specific capital costs range from $8,900 to over $246,000/kW$_e$.

When utilizing AGS for direct-use heating, competitive LCOH values are obtainable; however, these LCOH results are based on generous assumptions for financing, maintenance, drilling costs and surface

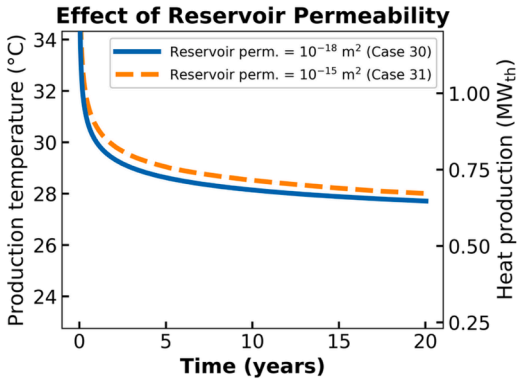

Fig. 18. Simulation results of U-loop AGS with natural convection in the reservoir for different levels of reservoir permeability. The low-permeability case (Case 30) corresponds to the conduction-only scenario. Increasing the reservoir permeability to 10^{-15} m^2 (Case 31) only slightly increases the thermal performance. All cases assume a U1-loop configuration with lateral length of 2 km, reservoir temperature of 120°C at 2 km depth, insulated injection and production well, and water as heat transfer fluid with flow rate of 20 $kg{\cdot}s^{-1}$ and injection temperature of 20°C.

equipment costs. In addition, the low production temperatures may limit the type of applications that can utilize the thermal energy effectively. Coupling an AGS with a heat pump system may be required to boost the supply temperature needed for certain applications. LCOE values for power production with AGS appear high. However, we only evaluate six electricity cases; lower values could be obtained for different geometries, designs and operation conditions. Relatively high LCOE values for AGS systems may be partially compensated by certain benefits such as the ability to provide power on demand, or avoiding the need to handle brine at the surface. Values for AGS capital cost and levelized cost are highly dependent on drilling costs. For example, for the U-loop scenarios, if the horizontal laterals can be drilled at $200/m instead of $1,000/m, a considerable reduction in costs and levelized costs is obtained, with the LCOH decreasing when adding more laterals (see Case 14, 26 and 27). The LCOH and LCOE values we calculate are for new AGS plants. Avoiding drilling new wells by repurposing idle or abandoned wells would significantly lower AGS capital and levelized costs.

4.6. Comparison of AGS with Existing Geothermal Systems

We now compare techno-economic performance of AGS with reported data from existing geothermal (hydrothermal) systems. Our AGS base case co-axial and U-loop scenarios (Cases 1 and 14) with a reservoir temperature in the range 150 to 200°C at 2 km depth, yield long-term production temperatures in the range 25 to 50°C with a flow rate of 20 $kg{\cdot}s^{-1}$, corresponding to average heat production of ~0.6 to ~2.1 MW_{th} (see Fig. 3 and 10). In comparison, existing hydrothermal plants appear to obtain superior thermal performance. For example, based on monthly production reports for 19 geothermal plants in California and Nevada, Snyder et al. (2017) report typical production temperatures of ~150°C, average flow rates of ~110 $L{\cdot}s^{-1}$ for binary plants and ~60 $L{\cdot}s^{-1}$ for flash plants, and thermal drawdown on the order of only ~1°C per year. The corresponding thermal output is on the order 10 to 50 MW_{th} per well doublet. In a first-order analysis, thermal performance with EGS is governed by the mass flow rate per heat transfer area (Armstead and Tester, 1987). A successful EGS fracture network may obtain a value of ~$2{\cdot}10^{-5}$ $kg{\cdot}s^{-1}{\cdot}m^{-2}$ or smaller for this metric, resulting in limited thermal drawdown over a 20-year lifetime. In contrast, with AGS, constraining the flow in a pipe places a limitation on the attainable flow rate per heat transfer area, resulting in rapid drawdown and limited thermal output. For example, our base case U-loop scenario (Case 14) has a mass flow rate per heat transfer area of ~$5{\cdot}10^{-3}$ $kg{\cdot}s^{-1}{\cdot}m^{-2}$.

Based on LCOH and LCOE values for hydrothermal plants, greenfield AGS appears expensive, particularly for electricity production. When utilizing AGS for direct-use heating, we find a base case LCOH value of $37/MWh and $52/MWh for co-axial and U-loop AGS, respectively (see Table 20). Beckers et al. (2021) and Robins et al. (2021) report LCOH values for existing geothermal district heating plants in the U.S. in the range $15 to $105/MWh. However, these levelized cost values assume more conservative economic and financing assumptions, and incorporate the cost for the surface district heating network. Our base case LCOE value when utilizing AGS for electricity is $1,315/MWh and $825/MWh, for co-axial (200°C at 2 km depth) and U-loop (150°C at 2 km depth), respectively (Table 21). However, lower LCOE values are obtained for higher reservoir temperatures, a larger number of laterals or when developing AGS in existing wells. For example, a U2-loop system developed in a reservoir of 500°C at 2 km depth with an aggressive $200/m horizontal lateral drilling cost (Case 40) results in an LCOE of ~$83/MWh. A forthcoming paper indicates that, at $200/m horizontal drilling cost, the LCOE can be further reduced when considering deeper systems and increasing the number of laterals. For hydrothermal systems, the *GeoVision* report estimates a supply curve for the United States with LCOE values in the range $60 to $80/MWh for several 1,000's of MW_e in installed geothermal capacity.

5. CONCLUSIONS

Through a series of 40 simulated case scenarios, our analysis provides a systematic evaluation of the technical performance and potential cost-competitiveness of co-axial and U-loop "advanced geothermal systems" (AGS) for heat and electricity production over a 20-year lifespan. By considering a range of different AGS designs and geometries, reservoir characteristics, and operating conditions, our results provide insight into the influence of these parameters and can help guide development decisions.

Based on our simulations, for reservoirs with temperatures ranging from 150 to 300°C at a 2 km depth (which correspond to relatively high average geothermal gradients, from 65 to 140°C·km^{-1}), thermal outputs are expected in the range 0.4 to 0.9 MW_{th} for a 2 km vertical co-axial system and from 1.3 to 4.5 MW_{th} for a 2 km deep U-loop with two laterals of 2 km length each (Fig.s 3 and 10).

Heat extraction rates from closed loop systems in conduction-dominated reservoirs are limited because of two underlying reasons: 1) the inherently low thermal conductivity (~1–5 $W{\cdot}m^{-1}{\cdot}K^{-1}$) and diffusivity of the rock (~10^{-6} $m^2{\cdot}s^{-1}$ of rock), which controls the heat flux through the rock zone surrounding the wellbore, and 2) the restricted contact area between the fluid and the rock mass as a result of confining the fluid in sealed wells. Larger thermal outputs are obtainable with higher reservoir temperatures, or through more well contact area with the rock, e.g., with a long horizontal extension for a co-axial system (Fig. 12) or with multiple laterals in a U-loop configuration (Fig. 16). In general, utilizing low injection temperatures and/or large mass flow rates tends to benefit heat production, particularly for U-loop systems (Fig. 14). Natural or forced convection increases output but requires relatively high reservoir permeability or Darcy velocities to have a considerable impact. For in-situ reservoir permeability of 10^{-15} m^2 (~1 mD), a common natural permeability found at depths of 2 to 4 km, we find only a moderate increase in thermal output due to natural convection (Fig.s 17 and 18).

For all the cases considered in this study, the thermal output and production temperature results reveal a characteristic behavior of reaching a peak during the first few hours of operation, but then quickly dropping and converging to a long-term steady value much lower than the initial reservoir temperature. With initial rock temperatures ranging from 150 to 300°C and fluid mass flow rates ranging from 10 to 40 $kg{\cdot}s^{-1}$, production temperatures for most cases decline to values of 20 to 60°C after a few hours, which are suitable for some direct-use applications and, if necessary, could be boosted to higher utilization

temperatures with heat pumps. Under these conditions, production temperatures are too low to efficiently produce electricity with a heat-to-power conversion cycle. Production temperatures can be increased when operating at very low flow rates, in very hot rock reservoirs, or in systems with extensive total lengths of the heat exchangers in the reservoir.

For our base case reservoir conditions (150 to 200°C at 2 km depth), we find that utilizing supercritical CO_2 (sCO_2) as the working fluid to directly drive a turbine for generating electricity appears more effective than utilizing water driving an ORC power plant. For example, for the U-loop design with two laterals 2 km long at 2 km depth and 150°C reservoir temperature, electricity production with sCO_2 is on the order of 90 kW_e, while with water driving an ORC plant, average electricity production is only about 50 kW_e. However, with much higher reservoir temperatures (e.g., Cases 37 and 40 with 500°C at 2 km), we find higher levels of electricity production using water rather than sCO_2.

Drilling costs significantly impact the total capital cost of AGS. For example, assuming a 50% reduction in drilling costs from the 2019 *GeoVision* report's baseline values for co-axial wells and the vertical wells in a U-loop system and $1,000/m for horizontal laterals, specific capital costs for most direct-use cases fall in the range of $2,000 to $8,000/$kW_{th}$ (Table 20). Assuming a 5% discount rate and 100% utilization rate, typical LCOH values fall in the range of $20/MWh to $60/MWh (Table 20). For the six electricity cases considered, LCOE values range from $83/MWh (for $200/m horizontal lateral drilling cost) to over $2,000 per MWh (Table 21). Lower levelized cost values may be obtainable after further optimizing the design or for other AGS configurations and geometries not investigated in our study. A forthcoming paper indicates LCOE values under $60/MWh may be obtainable for a 12-lateral 7-km deep U-loop type system with geothermal gradient of 60°C/km, in case the laterals can be drilled at $200/m. Similarly, repurposing existing idle or abandoned wells with AGS could be developed at a fraction of the cost calculated here, as our analysis only considers systems that require drilling of new wells. Nevertheless, because of typically low production temperatures, considering AGS for direct-use heat production first rather than for electricity generation appears to be preferable.

Comparison of AGS with EGS for low-permeability reservoirs indicates that, for greenfield sites, EGS reservoirs can supply larger thermal output with less thermal drawdown, but only if a fracture network can be established with sufficiently large heat transfer area without short circuiting or fluid flow channeling. If pre-existing reservoir permeability is sufficiently large to achieve economic flow rates through a large enough volume, one might first consider the option to develop a traditional or "hydrothermal" reservoir. Nevertheless, several situations have been identified where AGS could be a feasible option. Challenging subsurface conditions (e.g., aggressive fluid chemistry or presence of non-condensable gases) may prevent production of brine to the surface, leaving a closed-loop system as the preferred option. The same is true for extracting heat from formations with low permeability that cannot be stimulated (e.g., because of technical, legal or permitting limitations). In certain developed fields, more brine production could result in too much pressure drawdown in the reservoir, or could surpass the production cap as stipulated in the lease. In these situations, AGS could enable the production of more heat from the reservoir without producing additional fluid.

In summary, we find that AGS or closed-loop geothermal systems are plagued with low thermal performance, due to limited contact with the rock for heat exchange, and slow heat transfer rates within the rock. These limitations can partially be mitigated by targeting very high temperatures, and through multiple laterals, to increase contact area, however, the cost and complexity of multiple-loop systems quickly increase. For AGS requiring new wells to be drilled, we estimate relatively high levelized costs of energy, especially for electricity production, unless significant reductions in drilling costs can be obtained. Hence, AGS may be more appropriate when traditional hydrothermal is off the table, and in situations with existing wells. Also, to increase AGS energy output and lower levelized cost, considering first direct-use heating as end-use is recommended.

CRediT authorship contribution statement

Koenraad F. Beckers: Investigation, Formal analysis, Software, Writing – review & editing. **Nicolás Rangel-Jurado:** Investigation, Formal analysis, Software, Writing – review & editing. **Harish Chandrasekar:** Investigation, Formal analysis, Software, Writing – review & editing. **Adam J. Hawkins:** Supervision, Writing – review & editing. **Patrick M. Fulton:** Supervision, Writing – review & editing. **Jefferson W. Tester:** Supervision, Writing – review & editing.

Declaration of Competing Interest

The authors declare that they have no known competing financial interests or personal relationships that could have appeared to influence the work reported in this paper.

Acknowledgments

The authors acknowledge the partial support of Cornell University's College of Engineering and the Cornell Energy Systems Institute. The authors would like to thank Steve Beyers, Olaf Gustafson, Terry Jordan, Donald Koch, Ivan Purwamaska, Henry Johnston and Kate Young for providing valuable insights and feedback on closed-loop geothermal systems, and modeling with SBT and COMSOL. The views expressed in this paper belong solely to the authors.

APPENDICES

A.1 Description of SBT model

The SBT tool is a transient heat transfer simulator for modeling heat extraction with closed-loop geothermal systems in conduction-only or forced-convection geothermal reservoirs. The tool was originally developed by Beckers et al. (2015) to simulate computationally-fast transient heat transfer of slender bodies (e.g., a geothermal well) in conductive-only media. The theory was derived by asymptotically matching an infinite cylinder as inner solution to a finite line source as outer solution. Heat transfer of the slender body with the medium was coupled to fluid flow inside the slender body to allow simulating heat extraction with heat exchangers, such as shallow or deep closed-loop geothermal systems. The SBT model captures curvature of and thermal interaction between slender bodies, allows for varying injection temperature and fluid flow rate, and can handle both short and long time-scales. An initial rock temperature gradient is allowed but rock properties are required to be constant, isotropic and uniform. Options are available to lift some of these constraints (Beckers et al., 2015), but these are not currently considered.

The SBT model was numerically implemented in MATLAB by discretizing the heat exchanger into a set of straight pipe elements along the heat exchanger center line. The heat exchange at each pipe element is further discretized in time as a set of heat pulses that remain constant during each time step. Heat exchange between the fluid inside the heat exchanger and the surrounding rock depends on the temperature difference between the

fluid and contacting rock. The SBT model calculates the rock temperature along the heat exchanger using a hybrid approach. The temperature T at each pipe element i at the end of each time step m is the double summation of the temperature change due to all past and current heat pulses n (from 1 to m) from all pipe segments j (from 1 to N with N the total number of pipe elements):

$$T_{i,m} = \sum_{j=1}^{m} \sum_{n=1}^{m} \left(f_{i,j,m,n} \cdot Q_{j,n} \right)$$

with $Q_{j,n}$ the heat pulse at element j during time step n and $f_{i,j,m,n}$ the temperature change at element i at the end of time step m as a result of the heat pulse at element j during time step n. The factors $f_{i,j,m,n}$ are calculated using analytical equations for a cylindrical (infinite or finite), line (infinite or fine) or point source. Decision trees were developed based on non-dimensional numbers reflecting the time and length scales, to calculate $f_{i,j,m,n}$ accurately with the most simple (i.e., computationally-fast) model (Beckers et al., 2015).

The original SBT model assumed heat conduction-only in the reservoir, and water with constant thermo-physical properties as heat transfer fluid in a U-loop type heat exchanger. For this project, updates were made to the SBT model to allow for simulating different heat transfer fluids, variable fluid properties as a function of temperature and pressure, co-axial type heat exchangers, and reservoirs with uniform one-dimensional flow resulting in heat convection in addition to conduction. Following the approach used in several geothermal wellbore simulators (Ortiz-Ramirez, 1983; Bjornsson, 1987; Aunzo and Bjornsson, 1991; Chadha et al., 1993; Hasan and Kabir, 2010), steady-state conservation of mass, momentum and energy is applied to simulate temperature and pressure of the heat transfer/working fluid along the heat exchanger. We assume single-phase flow and no phase transitions. Conservation of momentum results in an expression for the pressure gradient as a result of friction, and changes in kinetic and potential energy:

$$-\frac{dp}{dz} = \frac{f\rho v^2}{2d} + \frac{d}{dz}\left(\rho v^2\right) + g\rho\sin(\theta)$$

with p the fluid pressure [Pa], z the local coordinate axially along the heat exchanger in the direction of flow [m], f the Darcy friction vector [-], ρ the fluid density [kg·m^{-3}], v the fluid velocity [m·s^{-1}], d the hydraulic diameter of the pipe [m], g the gravitational acceleration [9.81 m·s^{-2}], θ the local angle between direction of fluid flow and the horizontal reference (i.e., for flow upwards a vertical well, θ is 90°; for flow downwards a vertical well, θ is -90°). In case of turbulent flow, the Colebrook-White equation is used to calculate f (Fox et al., 2004). Combining conservation of mass and energy yields:

$$\dot{m}\frac{d}{dz}\left(h + \frac{v^2}{2}\right) + \dot{m}g\sin(\theta) = -Q$$

with $\dot{m}$ the fluid mass flow rate [kg·s^{-1}], h the specific enthalpy [J·kg^{-1}], and Q the heat exchange with the surroundings [W·m^{-1}]. Q is defined as being positive when heat is transferred from the fluid to the rock. For heat exchange between the fluid in a U-loop pipe or in the annulus of a co-axial pipe and the surrounding rock, Q is calculated as:

$$Q = \frac{T_f - T_r}{R_t}$$

with T_f the fluid temperature [°C], T_r the rock temperature in contact with the heat exchanger [°C], and R_t the thermal resistance [W·m^{-1}·K^{-1}]. The heat exchange is assumed positive if heat is transferred from the fluid to the rock, and negative in reverse. For fluid flow in a pipe in direct contact with the rock, R_t is calculated as:

$$R_t = \frac{1}{2\pi r_i h} + \frac{1}{2\pi k}\ln\left(\frac{r_o}{r_i}\right)$$

with h the convective heat transfer coefficient [W·m^{-2}·K^{-1}], k the thermal conductivity of the pipe wall material [W·m^{-1}·K^{-1}], r_i the inner radius of the pipe [m] and r_o the outer radius of the pipe [m]. Nusselt correlations are used for developed flow through a pipe to calculate h (Cengel, 2014). In case of different layers of thermal resistance (e.g., cement, tubing, vacuum insulation, etc.), additional terms are considered in the equation for R_t, to account for the thermal resistance in each layer. For a co-axial heat exchanger, similar expressions are used for Q and R_t to account for heat transfer between the fluid in the center pipe and the annulus.

Specific enthalpy and thermo-physical properties (e.g., density, viscosity) of the fluid are calculated as a function of temperature and pressure using the CoolProp open-source libraries (Bell et al., 2014). Fluid temperature, pressure, velocity and properties, as well as rock temperature and heat transfer between the heat exchanger and the rock and, for a co-axial heat exchanger, between the annulus and center-pipe, are coupled and solved iteratively at each time step. Long-term AGS performance in the presence of uniform water flow in the reservoir is simulated by replacing the point source and line source with the moving point and moving line source model Molina-Giraldo et al., (2011).

A.2 Validation of SBT and COMSOL models with Ramey's analytical wellbore heat transmission solution

To ensure that the SBT and COMSOL models were yielding accurate results, several validation cases were performed using both simulators. One such validation was a comparison with the wellbore heat transmission model by (Ramey, 1962). Ramey derived an analytical solution for the fluid temperature over time within a wellbore undergoing heat exchange with the surrounding rock. The solution assumes constant fluid and rock properties and no phase change in the well, and is only valid at long time scales (i.e, the thermal diffusion length must be significantly larger than the well radius). Ramey's solution for the fluid temperature in a well as a function of time and position is:

$$T(z,t) = T_o + az - aA + \left(T_{(i)}(t) + aA - T_{(o)}\right)e^{(-z/A)}$$

where z [m] is the position along the well in the direction of fluid flow (with $z = 0$ at well inlet), t is the time [s], a the geothermal gradient [°C·m^{-1}] (a is positive for injection wells with $z = 0$ at the surface and negative for production wells with $z = 0$ at the bottom of the well), T_o is the rock temperature at the inlet [°C], T_i the fluid temperature at the well inlet [°C], and A a function [m^{-1}] calculated as:

$$A = \frac{\dot{m} C_{p,f} \left(k_r + r_i U f(t)\right)}{2\pi r_i \, U k_r}$$

where $\dot{m}$ is the mass flow rate of fluid in the well [kg·s^{-1}], $C_{p,f}$ the fluid specific heat capacity at constant pressure [J·kg^{-1}·K^{-1}], k_r the rock thermal conductivity [W·m^{-1}·K^{-1}], r_i the tubing inner radius [m], U the overall heat transfer coefficient between inside of the tubing and outside of the casing [W·m^{-2}·K^{-1}], and $f(t)$ a time function capturing the transient heat conduction in the formation. In certain cases (e.g., water in liquid phase in geothermal wells without insulated tubing), thermal resistance in the wellbore is negligible and A can be simplified as:

$$A = \frac{\dot{m} \, C_{p,f} \, f(t)}{2\pi k_r}$$

At long enough time scales (i.e., typically after a week), $f(t)$ can be estimated assuming an infinite constant heat flux line source. The corresponding equation for long times is:

$$f(t) = -ln\left(r_{co} \Big/ \sqrt{4\alpha_r t}\right) - 0.29$$

with r_{co} is the casing outer radius [m] and α_r is the rock thermal diffusivity [m^2·s^{-1}].

A test simulation was constructed for a 7 km long pipe in an infinite medium. The rock was initially at a uniform temperature of 100°C (i.e., no geothermal gradient). The well was modeled as open-hole with radius of 0.0762 m, thermal conductivity of the rock is 2.83 W·m^{-1}·K^{-1} and thermal diffusivity were set at 1.2×10^{-6} m^2·s^{-1} respectively. Water at 50°C was injected at 10 kg·s^{-1}. The outlet temperature as a function of time was estimated with the Ramey equation and showed excellent agreement with the results of the SBT and COMSOL models (Fig. A1). The SBT model discretized the pipe in 70 elements of 100 m length each. The COMSOL model assumed a two-dimensional axisymmetric setup with logarithmically spaced mesh in the radial direction (i.e., element size grows in radial direction away from the pipe).

A.3 Validation of SBT and COMSOL models for Co-axial AGS cases

Several co-axial cases analyzed in Section 4.1 (heat conduction-only) were run both with the SBT and COMSOL models to validate the results. Production temperatures simulated with these models for cases 1 through 3 and cases 7 through 9 are shown in Fig. A2, indicating excellent agreement. Specifications for each case (e.g., reservoir temperature, fluid flow rate, etc.), were provided in Section 4.1.

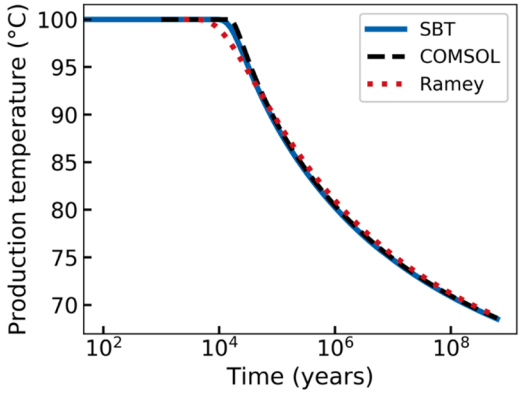

Fig. A1. Outlet temperature for test case calculated with Ramey, SBT model, and COMSOL. Test case considers a 7 km long pipe in rock medium initially at uniform temperature of 100°C, with water injected at 50°C.

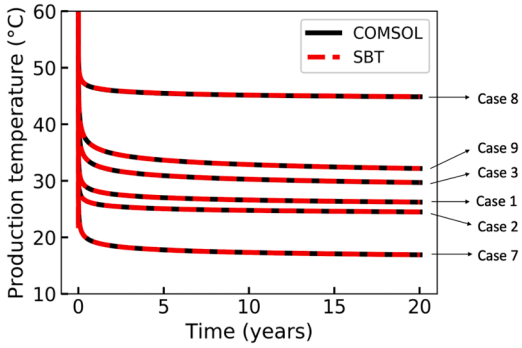

Fig. A2. Comparison of production temperature simulated with COMSOL and SBT model for co-axial AGS Cases 1 through 3 and 7 through 9 (see Section 4.1), indicating excellent agreement in results.

A.4 Validation of SBT and COMSOL models for U-Loop configuration with one lateral section

The SBT and COMSOL models for the U-loop configuration were compared with the Ramey heat transmission analytical solution (Appendix A2), applied sequentially to the injection well, horizontal lateral, and production well. The test case resembles Case 12 in Table 1 but with one lateral instead of two laterals. The U-loop is 2 km deep and the horizontal section is 2 km long. The surface temperature is 20°C and the reservoir temperature at 2 km depth is 150°C. The well was modeled as an open-hole channel with a radius of 0.1524 m. Water is injected at 20°C and 20 $kg{\cdot}s^{-1}$. The thermal conductivity of the rock was set to 2.83 $W{\cdot}m^{-1}{\cdot}K^{-1}$ and the thermal diffusivity is $1.2{\times}10^{-6}$ $m^2{\cdot}s^{-1}$. The COMSOL model considers a full three-dimensional set up with roughly 7.4 million tetrahedral mesh elements. Production temperature calculated with SBT, COMSOL and Ramey is plotted in Fig. A3, indicating good agreement between the three models. The Ramey solution predicts a slightly higher production temperature (~0.2°C) because thermal interference between the lateral and vertical wells at the two 90° bends is not accounted for.

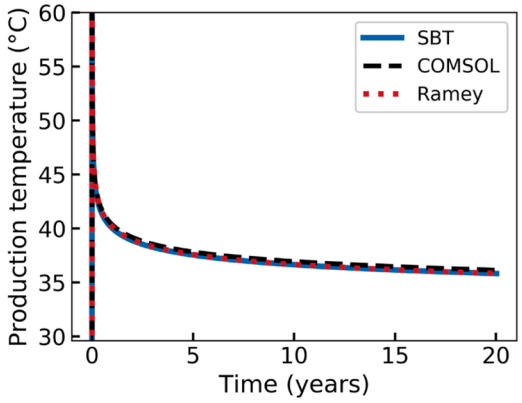

Fig. A3. Comparison of production temperature with SBT model, COMSOL model, and Ramey for single U-loop configuration, indicating good agreement between results.

A.5 Van Oort et al. (2021) U-loop configuration

Using the SBT model, we conducted a long-term simulation for the AGS design considered by Van Oort et al. (2021). The system was a U-loop configuration with two 7 km deep vertical wells and one 7 km long horizontal lateral. The reservoir temperature at 7 km depth was 222°C and the geothermal gradient was $26°C{\cdot}km^{-1}$. We assumed both the injection well and the horizontal lateral to be open-hole with a constant radius of 0.1129 m. The vertical producing well is vacuum insulated with a constant radius of 0.1129 m. Water is injected at 50°C with a flow rate of 97.2 $kg{\cdot}s^{-1}$. The thermal conductivity of the rock was 2.5 $W{\cdot}m^{-1}{\cdot}K^{-1}$, density was 2700 $kg{\cdot}m^{-3}$ and specific heat capacity was 1000 $J{\cdot}kg^{-1}{\cdot}K^{-1}$. We assumed the two 90° bends have a radius of curvature of 100 m. A large injection pressure of 100 bar was considered to ensure no flashing occurs of the water. Production temperature and heat production as a function of time were plotted in Fig. A4. The left-hand side figures were plotted with a logarithmic time-scale; the right-hand figures are plotted in linear time-scale. An initial peak of 220°C and 70 MW_{th} during the first few hours matches the results obtained by Van Oort et al. (2021). However, when running a multi-year simulation with constant 97.2 $kg{\cdot}s^{-1}$ flow rate, the production temperature quickly dropped to around 70°C and the heat production dropped to about 5 MW_{th}.

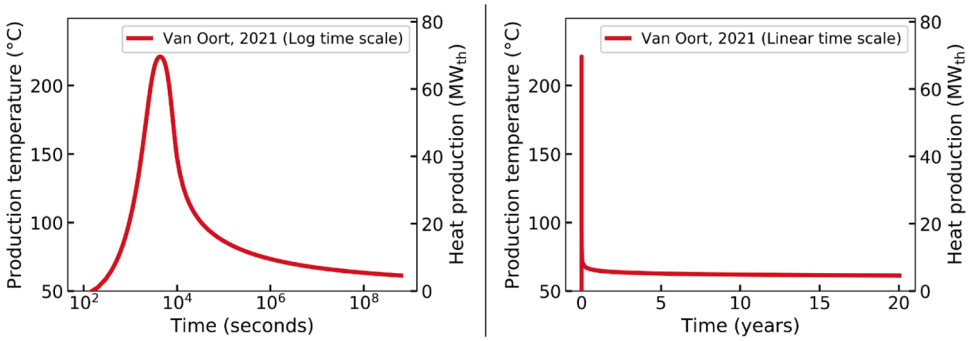

Fig. A4. Production temperature (in°C) and heat production (in MW_{th}) as a function of time (plotted in logarithmic time scale on the left-hand side and linear time scale on the right-hand side) for the Van Oort et al. (2021) U-loop configuration. Although heat production over 50 MW_{th} is obtained during the first few hours of operation, the long-term heat production over 20 years settles around 5 MW_{th}.

References

Amaya, A., Scherer, J., Muir, J., Patel, M., Higgins, B., 2019. (2020). GreenFire Energy Closed-Loop Geothermal Demonstration using Supercritical Carbon Dioxide as Working Fluid. Proceedings, 45th Workshop on Geothermal Reservoir Engineering. Stanford University, Stanford California. February 10-12.

Armstead, H.C.H., Tester, J.W., 1987. Heat Mining. E. & F.N. Spon Ltd., London and New York.

Beckers, K., 2016. Low-temperature geothermal energy: systems modeling, reservoir simulation, and economic analysis. Doctoral dissertation. Cornell University, Ithaca, New York.

Beckers, K.F., Koch, D.L., Tester, J.W., 2015. Slender-body theory for transient heat conduction: theoretical basis, numerical implementation and case studies. Proceedings of the Royal Society A: Mathematical, Physical and Engineering Sciences, 471 (2184), 20150494.

Beckers, K.F., Kolker, A., Pauling, H., McTigue, J.D., Kesseli, D, 2021. Evaluating the feasibility of geothermal deep direct-use in the United States. Energy Conversion and Management, 114335.

Beckers, K.F., McCabe, K., 2019. GEOPHIRES v2.0: updated geothermal techno-economic simulation tool. Geothermal Energy 7 (1), 1–28.

Bell, I.H., Wronski, J., Quoilin, S., Lemort, V., 2014. (2014). Pure and pseudo-pure fluid thermophysical property evaluation and the open-source thermophysical property library coolprop. Industrial & Engineering Chemistry Research 53 (6), 2498–2508.

Bjornsson, G., 1987. A multi-feedzone geothermal wellbore simulator. MS Thesis. Lawrence Berkeley Laboratory, University of California.

Bobok, E., Tóth, A., Turzó, Z., 2007. Sustainable Production of a Closed Loop Geothermal Well. GRC Transactions 31, 2007. Available at: http://pubs.geothermal-library.org/lib/grc/1025219.pdf.

Carlson, M D, Middleton, B M, Ho, C K, 2017. Techno-economic comparison of solar-driven SCO2 Brayton cycles using component cost models baselined with vendor data and estimates. Energy Sustainability, vol. 57595. American Society of Mechanical Engineers p. V001T05A009.

Cengel, Y., 2014. Heat and mass transfer: fundamentals and applications. McGraw-Hill Higher Education.

Chadha, P.K., Malin, M.R., Palacio-Perez, A., 1993. Modelling of two-phase flow inside geothermal wells. Applied mathematical modelling 17 (5), 236–245.

Cheng, W.L., Li, T.T., Nian, Y.L., Wang, C.L., 2013. Studies on geothermal power generation using abandoned oil wells. Energy 59, 248–254.

COMSOL, 2019. COMSOL Multiphysics Reference Manual. Comsol, Inc., Burlington, MA, United States. Available at: https://doc.comsol.com/5.5/doc/com.comsol.help.comsol/COMSOL_ReferenceManual.pdf.

DOE - U.S. Department of Energy, 2019. GeoVision Report. U.S. Department of Energy available at: https://www.energy.gov/eere/geothermal/geovision.

Eavor (2021). Eavor-Lite Demonstration Project. Available at: https://eavor.com/about/eavor-lite.

Esmaeilpour, M., Korzani, M.G., Kohl, T., 2021. (2021). Performance Analyses of Deep Closed-loop U-shaped Heat Exchanger System with a Long Horizontal Extension. Proceedings, 46th Workshop on Geothermal Reservoir Engineering. Stanford University, Stanford, California. February 15-17.

Fox, D., Higgins, B., Energy, G., Emeryville, C.A., 2016. The Effect of Well Density on Resource Depletion for a Vertical Closed-Loop sCO2 Geothermal Well System. Geothermal Resource Council Transactions 40.

Fox, R.W., Pritchard, P.J., McDonald, A.T., 2004. Introduction to fluid mechanics, 6th ed. Wiley, New York.

Greengard, L., Rokhlin, V., 1987. A fast algorithm for particle simulations. Journal of computational physics 73 (2), 325–348.

Hasan, A.R., Kabir, C.S., 2010. Modeling two-phase fluid and heat flows in geothermal wells. Journal of Petroleum Science and Engineering 71 (1-2), 77–86.

Higgins, B., Muir, J., Scherer, J., Amaya, A., 2019. GreenFire Energy Closed-Loop Geothermal Demonstration at the Coso Geothermal Field. GRC Transactions 43. http://pubs.geothermal-library.org/lib/grc/1034139.pdf.

Hodgson, J.L., 1927. (1927). Examination of the problem of utilizing the Earth's internal heat. In: *Proceedings in* Section G of the British Association for the Advancement of Science at its Leeds Meeting. September 2.

Holmberg, H., Acuña, J., Næss, E., Sønju, O.K., 2016. Thermal evaluation of coaxial deep borehole heat exchangers. Renewable Energy 97, 65–76.

Horne, R.N., 1980. Design considerations of a down-hole coaxial geothermal heat exchanger. Transactions, Geothermal Resources Council 4.

Huttrer, G.W., 2020. Geothermal power generation in the world 2015-2020 update report. In: Proceedings World Geothermal Congress 2020, Reykjavik, Iceland. April 26 –May 2, 2020Available at. https://www.geothermal-energy.org/pdf/IGAstandard/WGC/2020/01017.pdf.

Ingebritsen, S.E., Manning, C.E., 2010. Permeability of the continental crust: dynamic variations inferred from seismicity and metamorphism. Geofluids 10 (1-2), 193–205.

Lowry, T., Finger, J., Carrigan, C., Foris, A., Kennedy, M., Corbet, T., Doughty, C., Pye, S., Sonnenthal, E., 2017. GeoVision Analysis Supporting Task Force Report: Reservoir Maintenance and Development. Sandia National Laboratories, Albuquerque, NM. SAND2017-9977.

Lund, J.W., Toth, A.N., 2020. Direct Utilization of Geothermal Energy 2020 Worldwide Review. In: Proceedings World Geothermal Congress 2020, Reykjavik, Iceland, April 26 –May 2, 2020. Available at: https://www.geothermal-energy.org/pdf/IGAstandard/WGC/2020/01018.pdf.

Malek, A.E., Adams, B., Rossi, E., Schiegg, H.O., Saar, M.O., 2021. Electric Power Generation, Specific Capital Cost, and Specific Power for Advanced Geothermal Systems (AGS). 46th Workshop on Geothermal Reservoir Engineering. Stanford University, Stanford, California. February 15-17, 2021.

MathWorks, Inc., 2020. MATLAB. Version 2020a. The Math Works, Inc. Computer Software. Available at: http://www.mathworks.com

Molina-Giraldo, N., Blum, P., Zhu, K., Bayer, P., Fang, Z., 2011. A moving finite line source model to simulate borehole heat exchangers with groundwater advection. International Journal of Thermal Sciences 50 (12), 2506–2513.

Morita, K., Tago, M., 1995. Development of the downhole coaxial heat exchanger system: potential for fully utilizing geothermal resources. GRC Bulletin 83–92. March 1995Available at: http://pubs.geothermal-library.org/lib/grc/7002528.pdf.

Morita, K., Tago, M., Ehara, S., 2005. Case studies on small-scale power generation with the downhole coaxial heat exchanger. In: Proceedings, World Geothermal Congress, Antalya, Turkey, 24-29 April, 2005. Available at: https://www.geothermal-energy.org/pdf/IGAstandard/WGC/2005/1622.pdf.

Nalla, G., Shook, G.M., Mines, G.L., Bloomfield, K.K., 2005. Parametric sensitivity study of operating and design variables in wellbore heat exchangers. Geothermics 34 (3), 330–346. https://doi.org/10.1016/j.geothermics.2005.02.001 https://doi.org/.

Oldenburg, C., Pan, L., Muir, M., Eastman, A., Higgins, B.S., 2016. Numerical simulation of critical factors controlling heat extraction from geothermal systems using a closed-loop heat exchange method. In: Proceedings, 41st Workshop on Geothermal Reservoir Engineering, Stanford, California, February 22-24, 2016.

Ortiz-Ramirez, J., 1983. Two-Phase Flow in Geothermal Wells: Development and Uses of a Good Computer Code (No. SGP-TR-66). . Stanford University, Stanford, CA.

Ramey, H.J., 1962. Wellbore heat transmission. Journal of petroleum Technology 14 (04), 427–435.

Riahi, A., Moncarz, P., Kolbe, W., Damjanac, B., 2017. Innovative closed-loop geothermal well designs using water and super critical carbon dioxide as working fluids. In: Proceedings, 41st workshop on geothermal reservoir engineering. Stanford University, Stanford, California. February 13-15, 2017.

Robins, J., Kolker, A., Pauling, H., Beckers, K., Schmidt, B., Pettit, W., Flores-Espino, F., 2021. U.S. Geothermal Electricity and District Heating Market Report. U.S. Department of Energy Geothermal Technologies Program.

Rybach, L., Megel, T., Eugster, W., 2000. At what time scale are geothermal resources renewable? In Proceedings World Geothermal Congress 2000, Kyushu - Tohoku, Japan, May 28 - June 10, 2000, volume 2 867–873 pages.

Scherer, J., Higgins, B., Muir, J., Amaya, A., GreenFire Energy Inc., 2020. Closed-Loop Geothermal Demonstration Project. California Energy Commission. Publication. Number: CEC-300-2020-007.

Snyder, D.M., Beckers, K.F., Young, K.R., Johnston, B., 2017. Analysis of geothermal reservoir and well operational conditions using monthly production reports from Nevada and California. GRC Trans 41, 2844–2856.

Van Oort, E., Chen, D., Ashok, P., Fallah, H., 2021. Constructing Deep Closed-Loop Geothermal Wells for Globally Scalable Energy Production by Leveraging Oil and Gas ERD and HPHT Well Construction Expertise. In: Paper presented at the SPE/IADC International Drilling Conference and Exhibition, Virtual, March 2021. https://doi.org/10.2118/204097-MS https://doi.org/.

Vany, J., Hirschmiller, J., Toews, M., 2020. Subsurface Characterization Methods for Multilateral Closed Loop Geothermal Systems. Case Study of Field Scale Technology Demonstration Project in Alberta. In: Canada. Geothermal Resources Council Annual Meeting, Vol. 44, Davis, California.

Wang, G., Song, X., Shi, Y., Yang, R., Yulong, F., Zheng, R., Li, J., 2021. Heat extraction analysis of a novel multilateral-well coaxial closed-loop geothermal system. Renewable Energy 163, 974–986.

Wang, Z., McClure, M.W., Horne, R.N., 2010. Modeling study of single-well EGS configurations. In: Proceedings World Geothermal Congress 2010, 25, p. 29.

Xu, T., Hu, Z., Feng, B., Feng, G., Li, F., Jiang, Z., 2020. Numerical evaluation of building heating potential from a co-axial closed-loop geothermal system using wellbore–reservoir coupling numerical model. Energy Exploration & Exploitation 38 (3), 733–754.

Zhang, W., Wang, J., Zhang, F., Lu, W., Cui, P., Guan, C., Yu, M., Fang, Z., 2021. Heat Transfer Analysis of U-Type Deep Borehole Heat Exchangers of. Geothermal Energy. Energy and Buildings 237, 110794.

Robertson, E. C., 1988,*Thermal Properties of Rocks*. United States Geological Survey (USGS), Reston, VA. [Available from http://pubs.er.usgs.gov/publications/ofr88441].